REPORT DOCUMENTATION PAGE

Form Approved
OMB NO. 0704-0188

Public Reporting burden for this collection of information is estimated to average 1 hour per response, including the time for reviewing instructions, searching existing data sources, gathering and maintaining the data needed, and completing and reviewing the collection of information. Send comment regarding this burden estimates or any other aspect of this collection of information, including suggestions for reducing this burden, to Washington Headquarters Services, Directorate for information Operations and Reports, 1215 Jefferson Davis Highway, Suite 1204, Arlington, VA 22202-4302, and to the Office of Management and Budget, Paperwork Reduction Project (0704-0188,) Washington, DC 20503.

1. AGENCY USE ONLY (Leave Blank)	2. REPORT DATE September 2, 2003	3. REPORT TYPE AND DATES COVERED
		Final June 1, 2000 to ~~August 30, 2003~~ 31 May 03

4. TITLE AND SUBTITLE	5. FUNDING NUMBERS
Physics of magnetic multilayers and devices at millimeter wave frequencies	Grant DAAD19-00-1-0146

6. AUTHOR(S)
Zbigniew J. Celinski
Robert E. Camley

7. PERFORMING ORGANIZATION NAME(S) AND ADDRESS(ES)	8. PERFORMING ORGANIZATION REPORT NUMBER
Department of Physics, University of Colorado at Colorado Springs 1420 Austin Bluffs Parkway Colorado Springs, CO 80918	

9. SPONSORING / MONITORING AGENCY NAME(S) AND ADDRESS(ES)	10. SPONSORING / MONITORING AGENCY REPORT NUMBER
U. S. Army Research Office P.O. Box 12211 Research Triangle Park, NC 27709-2211	41078.1-PH

11. SUPPLEMENTARY NOTES

The views, opinions and/or findings contained in this report are those of the author(s) and should not be construed as an official Department of the Army position, policy or decision, unless so designated by other documentation.

12 a. DISTRIBUTION / AVAILABILITY STATEMENT	12 b. DISTRIBUTION CODE
Approved for public release; distribution unlimited.	20030925 007

13. ABSTRACT (Maximum 200 words)

Microwave devices are widely used in both military and civilian communications systems. During the last decades, we have witnessed incredible progress in high frequency semiconductor electronics and, in particular, a movement towards the synthesis of different electronic components into integrated circuits. The obvious obstacle, however, to an increased use of microwave and millimeter wave technology is the lack of advances in magnetic structures at high frequencies, 10-100 GHz. The main goal of this project was to look at both fundamental and applied physics relating to high frequency (10-100 GHz) waves in magnetic materials and devices. We have developed three different signal processing devices:, tunable band stop and band pass filters and tunable phase shifters based on the ferromagnetic metals. We demonstrated operation of these devices at frequencies up to 30 GHz in low magnetic fields.

14. SUBJECT TERMS	15. NUMBER OF PAGES
microwave devices band stop filter band pass filter phase shifter	6
	16. PRICE CODE

17. SECURITY CLASSIFICATION OR REPORT UNCLASSIFIED	18. SECURITY CLASSIFICATION ON THIS PAGE UNCLASSIFIED	19. SECURITY CLASSIFICATION OF ABSTRACT UNCLASSIFIED	20. LIMITATION OF ABSTRACT UL

NSN 7540-01-280-5500

Standard Form 298 (Rev.2-89)
Prescribed by ANSI Std. 239-18
298-102

4) Statement of the problem studied

The main objective of our program was to develop a series of the microwave devices based on ferromagnetic metals. In particular, we developed processes, based on the sputtering technique, which allow us to make band stop and band pass filters and phase shifters. We have successfully accomplished this goal. We have also employed different schemes to increase operation frequency of our devices. In addition, we studied different materials which could allow us to boost the frequency response of our structure by employing the exchange bias or exchange coupling in layers structures. We describe a summary of our findings below.

5) Summary of the most important results

(a) Tunable Band stop filters

Tunable filters based on the ferrimagnetic dielectric YIG are a well-established technology that works well at lower frequencies. Band-stop or notch filters, for example, rely on ferromagnetic resonance (FMR) to absorb microwave power at the FMR frequency. This frequency, f, is set by material properties, such as saturation magnetization, M_s, anisotropy fields, H_a, the gyromagnetic ratio, γ, and the magnitude of an applied field, H. If the applied field is along the easy axis, the frequency is given by

$$f = \gamma\sqrt{(H + H_a)(H + H_a + 4\pi M_s)} \qquad (1)$$

and therefore the resonance frequency can be varied with an electromagnet. The maximum field produced by the electromagnet determines the upper limit for the band-stop frequency. For YIG with a low $4\pi M_s = 1.75$ kG and no anisotropy an applied field of over 11 kOe is necessary to reach frequencies of about 35 GHz. Such large fields are incompatible with devices of a limited size since substantial electromagnets are required. For Fe based devices one needs only field of 4.7 kOe to reach 35 GHz.

While Fe has a much higher resonance frequency for the same applied field, its conductivity can lead to high loss at microwave frequencies. However, structures utilizing thin Fe films minimize conduction loss while still producing high attenuation at the band-stop frequency. Early attempts at producing Fe-film-based structures succeeded in making filters with high band-stop frequencies and low broadband loss. However, the maximum attenuation only reached about 4–5 dB/cm.

Our theoretical calculations indicated that attenuation in the notch filters was inversely proportional to the thickness of the waveguide. Based on this work, we have recently constructed microstrip band-stop filters using a different geometry and growth method, resulting in much higher attenuation. Previous filter structures used epitaxial Fe films grown directly on semi-insulating GaAs wafers. The backside of the wafer and the Fe films were then coated with a high conductivity metal. The Fe side was then etched into a strip to form the microstrip structure. For these filters, high quality Fe with a linewidth of 35 Oe is required to get even a small attenuation. Our devices, in contrast, consist of layers deposited on only one
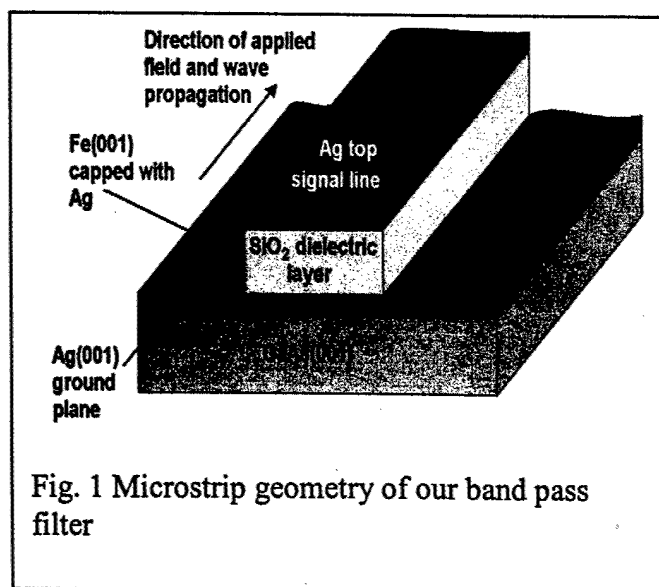

Fig. 1 Microstrip geometry of our band pass filter

side of a GaAs (001) wafer as shown in Fig. 1. This allows us to have a much thinner dielectric layer which ultimately results in a much higher attenuation. Most of the previous devices have been fabricated using Molecular Beam Epitaxy (MBE), a process which is not usually compatible with industrial techniques for mass production. In contrast, we have constructed magnetic devices grown by magnetron sputtering, a technique commonly used in industry. The sputtering technique has a second advantage. MBE grown films are generally thin, less than 100 nm, but the microwave devices often require films with thicknesses that are much larger, 1-2 microns. This is because the film thickness should be on the order of the skin depth in the magnetic material. The sputtering technique is quite capable of producing these thicker films.

In addition to the microstrip geometry we explored a new geometry – a coplanar waveguide (CPW). For this structure, illustrated in Fig. 2, we again used GaAs substrates. However, in this case also the sample was prepared in a sputtering system. We deposited either a Permalloy (Py) or Fe film on top of a thin Ta adhesion layer. The thicknesses of the magnetic layers were typically between 750nm and 1000 nm. The ferromagnetic layers were protected from oxidization with a thin Cu film. The films were patterned by photolithography followed by sputter etching in an Ar atmosphere. The lines were designed for a nominal characteristic impedance of 50 Ω. The waveguides made two right-angle bends to allow probes to contact from the sides, while a field was applied parallel with the length of the line. The lines are wide near the two ends to allow for probing but narrow in the middle to increase the magnitude of the resonance effects. Figure 2 shows a photograph of one right-angle bend and width transition, including dimensions.
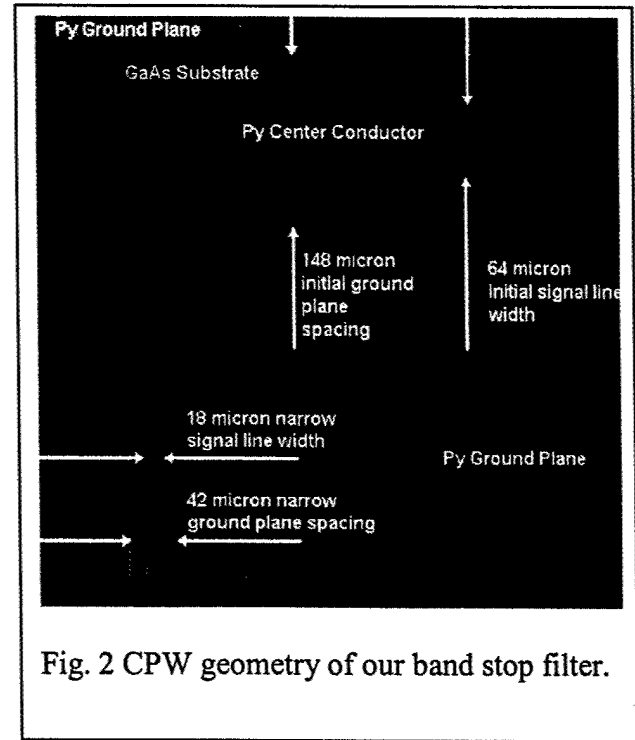

Fig. 2 CPW geometry of our band stop filter.

We characterized our structures from 0.5 to 40 GHz using an automated vector network-analyzer (VNA), and a micro-probe station; the on wafer calibration was done using the NIST Multical® software for the through-short-line (TRL) calibration procedure. The longest and the shortest lines used for calibration were 0.71 and 0.25 cm to cover the entire frequency range of interest.
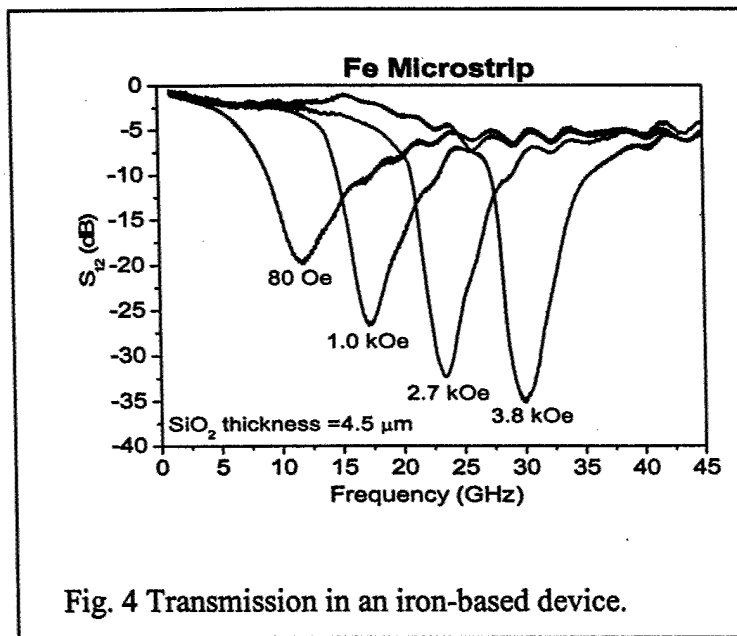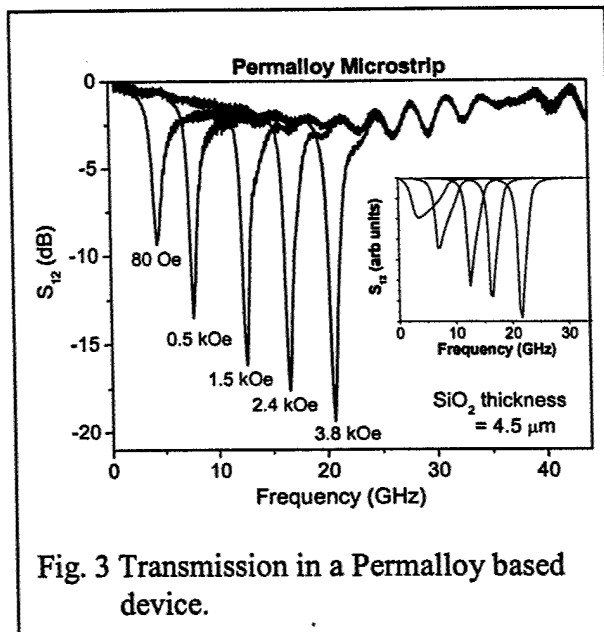
In Figure 3 we depicted an example of transmission as a function of frequency for the Py based microstrips. The insertion loss over most of the region is on the order of 2-3 dB while the power attenuation is close to values of 100 dB/cm. The width of the attenuation dip (measured at 3 dB above the minimum, i.e. half maximum) becomes distinctly narrower at higher frequencies (0.4 GHz for the dip at 20 GHz compared to a width of 0.82 GHz at 4.3 GHz). This narrowing of the width of the attenuation peak is consistent with our theoretical results as seen in the inset. In Figure 4 we show the results for an Fe based microstrip. For the Fe-based structure the insertion loss is somewhat larger, between 3-5 dB. The power attenuation is dramatically larger, 180 dB/cm at 30 GHz. Again we seen a narrowing of the width of the attenuation dip – it is 3 GHz at 11 GHz and narrows to 1.9 GHz at 30 GHz.

We have also found that we may use the effect of the shape anisotropy to increase the operational frequency. The magnetic material in our structure is in the form of a long ribbon with the following dimensions – length = 3 mm, width = 18 μm, thickness = 0.35 μm. This leads to the following dynamic demagnetizing factors, $N_x = 0.966$, $N_y = 0.034$, and $N_z = 0$. The formula for the resonance condition is now given by

$$f = \gamma\sqrt{\left(H + H_a + (N_y - N_z)4\pi M_s\right)\left(H + H_a + (N_x - N_z)4\pi M_s\right)} \qquad (2)$$
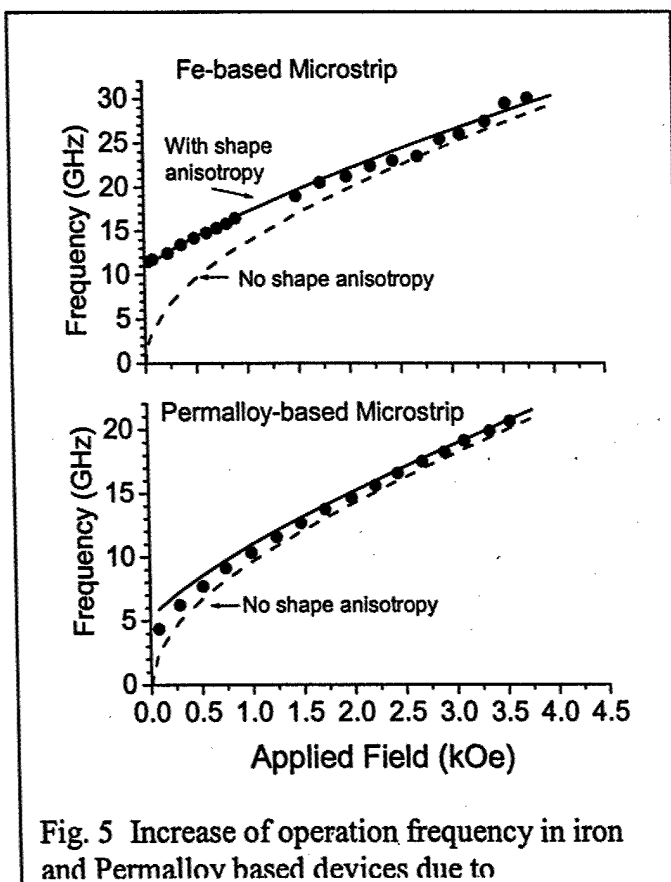
If we calculate the frequency at zero applied field, we find that without the shape anisotropy the frequency is zero (if $H_a = 0$) and with the shape anisotropy the frequency is about 11 GHz for the Fe structure and

about 5 GHz for Permalloy. This is a substantial boost in operational frequency which agrees very well with experimental data (see Figure 3 and 4.)

Fig. 3 Transmission in a Permalloy based device.

Fig. 4 Transmission in an iron-based device.

We show the dependence of the operational frequency on applied field in Figure 5. The dots represent the experimental results and the solid lines are the theoretical results based on Eq. (2) with no adjustable parameters. The dashed line represents the theoretical results in the absence of shape anisotropy. The effect of the shape anisotropy is clearly present in the experimental data, particularly at low magnetic fields. The effect is substantially larger in Fe than in Permalloy because the saturation magnetization in Fe is more than double that of Permalloy.

The same devices can also produce a phase shift, and we have characterized the phase shift in our microstrips as a function of the magnetic field. The attenuation of the signal in these devices, for each frequency, is below 3 dB. The results measured in the Fe-based microstrip are on the order of 360 deg/cm with an applied field of 1 kOe. The observed phase shift for the Permalloy-based devices was smaller, on the order of 100 deg/cm, again with a magnetic field of 1 kOe.

Fig. 5 Increase of operation frequency in iron and Permalloy based devices due to

The devices based on co-planar waveguide (CPW) geometry exhibited much smaller effects. From the measured scattering transmission matrix coefficients S_{21} we estimated the resonance insertion loss that for Fe-based CPW filter was ~ 35 dB/cm in the entire applied magnetic field range. In addition, the total insertion loss of the measured device has an additional non-magnetic insertion loss of 12 dB. In contrast, the transmission scattering matrix coefficient S_{21} for the Py-based CPW filter exhibited insertion loss for this filter is ~ 10 dB/cm with an additional non-magnetic insertion loss of ~ 7 dB.

In summary, we have prepared a series of the band stop filters using microstrip and co-planar geometries and employing ferromagnetic metals as an active element. The microstrip based devices exhibit superior properties (small insertion loss, very high attenuation) when compared to the co-planar device.

(b) Tunable band pass filter

We have constructed a novel band pass filter using a layered structure with at least two different magnetic materials. This filter works in the 5-50 GHz range with external magnetic fields of below 10 kG. The key idea is that each of the magnetic materials absorb electromagnetic waves at a different frequency. For example using Fe and Permalloy as the magnetic films and an external field of 2.5 kG one can have absorption bands centered at 17 GHz and 22 GHz. The region between these absorption bands has low attenuation and acts a band pass filter. This filter is tunable because an external magnetic field controls the position of the absorption bands.

One geometry for such a band pass filter is shown below (see Figure 6). The thicknesses of the Fe and Permalloy are critical – The Fe thickness must be relatively small to minimize eddy current effects and is typically on the order of 0.15 micrometers. Because the Permalloy has a narrower linewidth and lower conductivity the thickness of the Permalloy should be substantially thicker than the Fe, typically 0.4 micrometers. Initial experimental results for this structure are shown below.
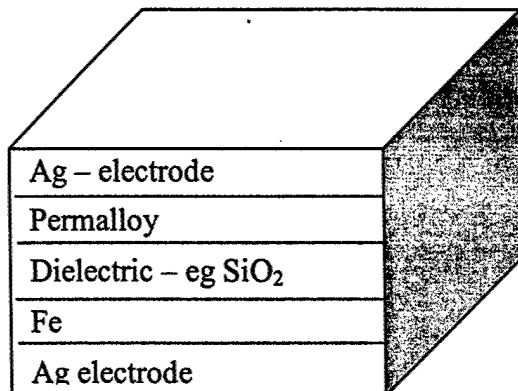

Fig. 6 Cross-section of the band pass filter

Fig. 7 Transmission vs. frequency for two different values of magnetic field

We also have theoretical calculations for this effect. Using the same parameters as discussed above we find the results shown in Figure 8. The between theory and experiment is excellent. Other geometries are also possible. One can include additional magnetic layers and dielectric layers to improve the transmission in the band pass region and extend the band stop regions. Coplanar waveguides using two different magnetic materials are also possible.

In summary, the band pass filter based on two ferromagnetic metals shows a lot of promise, however additional work is needed to refine its properties. In particular, one needs to decrease the insertion loss (currently at 6 dB) to a level of 3-4 dB at the band pass frequency.
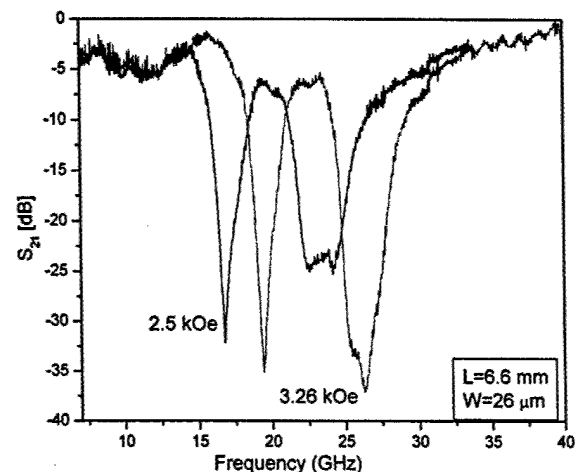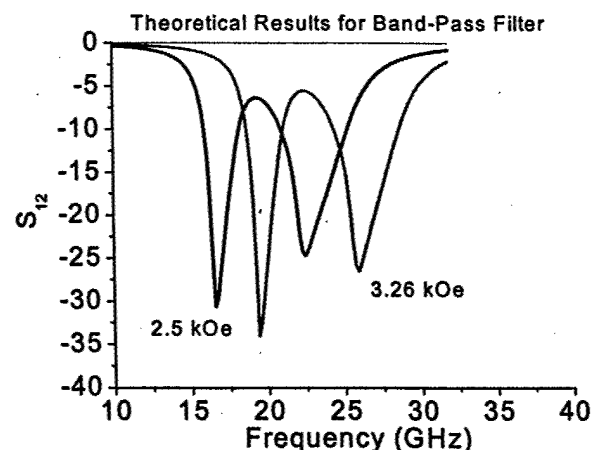

Fig. 8 Theoretical calculation for band pass filter.

6. Publications:

1. Bijoy Kuanr, L. Malkinski, R. E. Camley, Z. Celinski, and P. Kabos, "Iron and Permalloy based magnetic monolithic tunable microwave devices", J. Appl. Phys. **93**, 8591 (2003)
2. N. Cramer, D. Lucic, D.K. Walker, R.E. Camley, Z. Celinski, IEEE Trans. Magn., **37**, 2392 (2001)
3. Bijoy K. Kuanr, R. E. Camley, and Z. Celinski, "Exchange bias of NiO/NiFe. Linewidth broadening and anomalous spin –wave damping", J. Appl. Phys. **93**, 7723 (2003)
4. Bijoy K. Kuanr, M. Buchmeier, D.E. Buerger, P. Grnberg, R.E. Camley, and Z. Celinski, "Dynamic and Static measurements on epitaxial Fe/Si/Fe", J. Vac. Sci. Technol. July (2003)
5. J.P. Nibarger, R. Lopusnik, Z. Celinski, and T.J. Silva, "Variation of magnetization and the Landé g-factor with thickness in Ni-Fe films", Appl. Phys. Letter, **83**, 93 (2003)
6. N. Cramer, D. Lucic, R. E. Camley, Z. Celinski "High attenuation tunable microwave notch filters utilizing ferromagnetic resonance", J. Appl. Physics, **87**, 6911 (2000)
7. L. Malkinski, T. O'Keevan, R. E. Camley and Z. Celinski,L. Wee and R. L. Stamps, and D. Skrzypek, "Exchange bias in the $Fe/KCoF_3$ system –a comprehensive magnetometry study", J. Appl. Phys. **93**, 6835 (2003)
8. L. Malkinski, R. E. Camley, Z. Celinski, T.A. Winningham, S.G. Whipple, and K. Douglas, "Hexagonal Lattice of 10 nm Magnetic Dots", J. Appl. Phys. **93**, 7325 (2003)

Paper published in the Conference proceedings

9. N. Cramer, D.K. Walker," Modeling coplanar waveguide structures constructed of ferromagnetic metals", 2001 IEEE MTT-S International Microwave Symposium Digest (Cat. No.01CH37157), 2001, pt. 1, p 483-6 vol.1

Papers submitted for publications

10. Bijoy Kuanr, R. E. Camley, Z. Celinski, "High Frequency Band Stop Magnetic Filters" submitted to Applied Physics Letters

7. Personnel:

Nicolas Cramer	**– PhD student (PhD awarded in May of 2002)**
Dragan Lucic	**- MSc. Student**
Bijoy Kuanr	**- Post-doctoral associate**
Leszek Malkinski	**- Post-doctoral associate (currently assistant professor at the University of New Oreleans)**

8 Patents disclosure

A High Frequency Tunable Band Pass Filter Based on Thin Magnetic Films

By Z. Celinski and R.E. Camley

Modeling Coplanar Waveguide Structures Constructed of Ferromagnetic Metal*

Nicholas Cramer, *student member, IEEE*

Dept. of Physics, University of Colorado, Colorado Springs, CO, 80918, USA

David K. Walker, *member, IEEE*

National Institute of Standards and Technology, Boulder, CO, 80305-3328, USA

Abstract — We fabricate coplanar waveguide transmission lines with thin-film $Fe_{0.2}Ni_{0.8}$ conductors. These lines demonstrate a power attenuation of 10 dB/cm at ferromagnetic resonance frequencies of 5 to 10 GHz for applied magnetic fields less than 100 mT (1 kG). In addition, the phase of the transmitted wave can be tuned by about 20 degrees/cm by adjusting an applied magnetic field. We present a simple model for the complex reflected and transmitted waves as a function of material characteristics, geometry, and applied field. We model the skin effect influence on the transmission line circuit parameters, including the line impedance and propagation constant, by considering the full effects of the conductor permeability and conductivity.

I. INTRODUCTION

As communication applications progress to higher and higher operating frequencies, there is increasing demand for devices able to operate at these frequencies. Devices such as tunable filters and phase shifters have traditionally relied on ferrites such as YIG for their operation [1]. These devices function at, or close to, the ferromagnetic resonance (FMR) frequency, which is determined by material properties such as saturation magnetization (M_s) and by applied magnetic field. Due to their relatively low M_s, ferrimagnets require large magnetic fields in order to increase the resonance frequency above a few GHz.

Ferromagnetic metals such as Fe and permalloy (Py or $Fe_{0.2}Ni_{0.8}$) have much higher M_s and therefore their resonant frequencies are higher for a given applied field. The major drawback of these ferromagnetic metals is their high electrical conductivity. Ferrimagnets are insulators and have been engineered for decreased dielectric loss. Applying ferromagnetic metals in this way is clearly impractical. Instead, there have been various studies of devices constructed with the ferromagnet incorporated into a transmission line's conductive elements. The

theoretical treatment of such devices was explored by Schloemann and co-workers [2] and by Camley and Mills [3]. Previous studies have used a thin ferromagnetic film incorporated in the ground plane or signal conductor of a microstrip structure [4]-[6]. Our recent study [7] used a coplanar waveguide (CPW) constructed of Py conductors on a GaAs substrate.

II. THEORY

When modeling a line based on a magnetic dielectric, the task usually involves starting with a model that assumes perfect conductors and a relative permeability in the dielectric equal to unity. Next, the equations are modified to accommodate the complex, anisotropic permeability of the dielectric. As a final step, conduction loss in the conductors is added. In our case, the dielectric is non-magnetic and all magnetic effects enter the model via the skin effect in the conductors.

Modeling the skin effect is a two-step process. First, we extract the non-magnetic skin effect and second we modify it with the proper magnetic contribution. Extraction of the skin effect is aided by modeling the inductance and capacitance per unit length (L and C, respectively) by,

$$L = \mu_r \mu_0 g \qquad (1)$$

and,

$$C = \frac{\varepsilon_r \varepsilon_0}{g} \qquad (2)$$

where μ_r and μ_0 are the relative and free-space permittivities, respectively, ε_r and ε_0 are the relative and free-space permeabilities, respectively, and g is an unitless geometric factor that accounts for the device geometry. If we assume a lossless line with $\mu_r = 1$ (the usual

assumptions made in models of "normal" lines), we find that the impedance has the form,

$$Z_0 = \sqrt{\frac{g^2 \mu_0}{\varepsilon_r \varepsilon_0}} = \frac{g \eta_0}{\sqrt{\varepsilon_r}},$$ (3)

and hence g can easily be found using equations in the literature for Z_0 [8]. Next, we recognize that Z_0 is a function of skin depth as well as the material properties, μ_r and ε_r. Z_0 is a function of a, the signal line width, b, the ground plane spacing, t, the conductor thickness, and h, the substrate thickness. These dimensions are defined in the cross section shown in Fig. 1. If we correct a and b for the skin effect, we can construct two equations—one for Z_0, the zero skin depth impedance, and another for Z'_0, the finite skin depth impedance,

$$Z_0 = Z(a, b, t, h),$$ (4)

and,

$$Z'_0 = Z(a - \delta, b + \delta, t, h).$$ (5)

From these two impedances, two g's can be extracted (g and g', respectively). Note that:

$$g' - g = \Delta g > 0.$$ (6)

Now we propose that Δg represents the added influence of the skin depth region of the conductors and therefore we can express the modified inductance L' as:

$$L' = \mu g' = \mu_{dielectric} g + \mu_{eff} \Delta g,$$ (7)

where $\mu_{dielectric}$ is assumed to be μ_0 and μ_{eff} is an effective permeability in the ferromagnetic conductor (a complex quantity). Note that for non-magnetic conductors μ_{eff} is equal to $\mu_c(1 + j)$, where μ_c is the dc permeability of the metal, and that this formulation reduces to common expressions for L and R that account for the skin effect [9].

The next task is to derive expressions for the skin depth and μ_{eff}. First, note that μ in the conductor can be represented by the "Voigt permeability" (μ_{voigt}) [2],

$$\mu_{voigt} = \frac{\mu_1^2 - \mu_2^2}{\mu_1},$$ (8)

where,

$$\mu_1 = \mu_0 + \frac{\mu_0 \gamma_0 M_S (\gamma_0 B_0 - j\Gamma\omega)}{(\gamma_0 B_0 - j\Gamma\omega)^2 - \omega^2},$$ (9)

and

$$\mu_2 = \frac{\mu_0 \gamma_0 M_S \omega}{(\gamma_0 B_0 - j\Gamma\omega)^2 - \omega^2}.$$ (10)

B_0 is the applied magnetic field, γ_0 is the gyromagnetic ratio, and Γ is the damping factor. Schloemann [2] proposed that the complex scalar μ_{voigt}, instead of the entire permeability matrix, be used to model the interaction of EM waves with ferromagnets. The relevance of this approach was rigorously confirmed later by Astalos and Camley [10]. Also note that μ_{voigt} is not μ_{eff}—the former only includes magnetic effects and the latter must include both magnetic and electric (conduction) effects.

The skin depth and μ_{eff} both derive from the propagation constant of a wave in a ferromagnetic conductor:

$$\gamma = j\omega \sqrt{\varepsilon \mu_{voigt}},$$ (11)

where ω is the angular frequency. As is usual for a conductor,

$$\varepsilon \approx \frac{j\sigma}{\omega},$$ (12)

where σ is the conductivity. Hence, the skin depth as a function of frequency and applied field can be found for a ferromagnetic conductor with known conductivity and magnetic properties:

$$\delta = \frac{1}{Re(\gamma)}$$ (13)

Below, we derive an expression for μ_{eff} using the propagation constant. First, we follow the usual technique for determining surface impedance using a known propagation constant; that is, we integrate the surface current density due to an electric field and divide voltage by current. This results in a surface impedance per unit length of:

$$Z_s = \left(\frac{\delta}{w}\right) \frac{\gamma \, Re(\gamma)}{\sigma}$$ (14)

Recognizing δw as the geometric factor Δg for a parallel-plate structure, we write:

$$Z_s = \Delta g \frac{\gamma \, Re(\gamma)}{\sigma} = j\omega \Delta L$$ (15)

where $\Delta L = L' - L$ is the added inductance from (7) and therefore:

$$\mu_{eff} = \frac{\gamma \, Re(\gamma)}{j\omega\sigma} = \mu_{voigt} + j|\mu_{voigt}|$$ (16)

Knowing μ_{eff}, we refer to (7) and hence we now have an expression for the complex inductance (containing L and

484

R) per unit length. The capacitance per unit length is found via (2) and (3). The shunt conductance per unit length is easily found from the capacitance (given a known dielectric loss tangent) by considering a complex ε in (2)—this is not described in detail in this report.

Now that all four circuit parameters, R, L, C, and G, are known, the impedance and propagation constant of the line can be easily determined [9] and thus the complex scattering-parameter matrix as a function of frequency can be simulated [11].
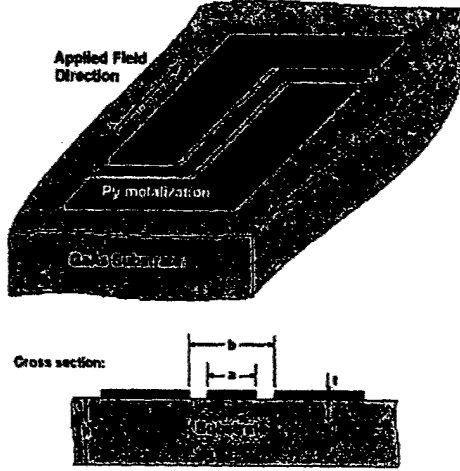

Fig. 1. Schematic of the CPW structure measured. Note the right-angle bends to allow probing from the sides and the applied field direction.

III. RESULTS

Fig. 1 shows the general construction of the line used for the measurements and simulations. The two right-angle bends allow the network analyzer probes to contact the line from either side while an electromagnet applies a field in the direction shown. The spacing between ground planes (b) is 148 μm and the width of the center signal line (a) is 64 μm. In our previous study, the structure also included a narrower region that was designed to increase the magnetic effects: this region has a larger skin depth relative to the conductor widths. For the material
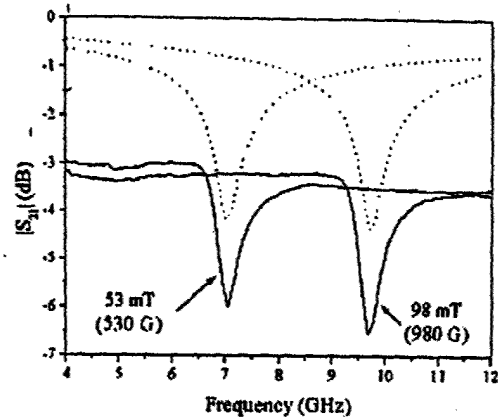

Fig. 2. Comparison between transmitted voltage magnitude experiment (solid lines) and simulation (dotted lines) for two different applied field values.
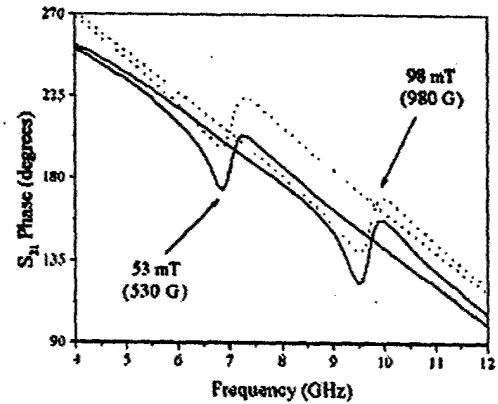

Fig. 3. Comparison between transmitted voltage phase experiment (solid lines) and simulation (dotted lines) for two different applied fields.

parameters, we used 850 kA/m for M_s, 180 GHz/T for γ_0 and $6.25 \times 10^5 \ \Omega^{-1} m^{-1}$ for σ.

Fig. 2 presents results demonstrating the tunable notch filter effect. Note that the solid experimental lines differ from the dotted simulation lines primarily because of additional background attenuation measured in the experiment. Note that, as expected, the notch frequency increases with applied field in accordance with the FMR frequency equation:

$$\omega = \gamma_0 \sqrt{B_0 \left(B_0 + \mu_0 M_s \right)} \qquad (17)$$

where γ_0 is the gyromagnetic ratio, B_0 is the applied field, and M_s is the saturation magnetization. The notch depth is

485

about 3 dB in voltage terms for a line length of 6.565 mm—this converts to about 10 dB/cm.

The phase shift effect occurs near the FMR frequency, as shown in Fig. 3. By changing the applied field, the phase of the transmitted wave can be increased or decreased continuously. For example, at 10 GHz the phase can be increased by about 15 degrees by increasing the field and moving the resonance frequency closer to 10 GHz. Considering that the line length is 6.565 mm, this translates to a phase-shift of about 20 degrees/cm. This effect is well approximated in the simulation (dotted lines), except that the experimental lines (solid lines) are shifted down by about 10 degrees.

IV. CONCLUSION

We present a simple model for CPW structures constructed of ferromagnetic conductors on a dielectric substrate. Unlike transmission lines with magnetic dielectrics, these structures demonstrate magnetic effects that occur only in the skin depth region of the conductive elements. Hence, we modify the circuit elements to account for skin depth and develop an expression for surface impedance that includes the magnetic effects. The result is a method for determining the impedance and propagation constant, given device geometry and magnetic properties. Our simulation of Py-based CPW lines approximates the magnitude and frequency position of the effects observed in our experimental measurements.

Transmission line structures based on ferromagnetic metals hold great promise for high-frequency applications. Our recent demonstrations of filters and phase-shifters based on these materials, along with this presentation of a model, increases the potential for future practical applications.

ACKNOWLEDGEMENT

REFERENCES

[1]   W. S. Ishak, "Magnetostatic wave technology: a review," Proc. IEEE, vol. 72, pp. 171-87, 1988

[2]   Ernst Schloemann, Randal Tustison, Jehoshua Weissman, H. Jerrold Van Hook, and Thomas Varitimos, " Epitaxial Fe films on GaAs for hybrid semiconductor-magnetic memories," J. Appl. Phys., vol. 63, pp. 3140-2, 1988

[3]   R. E. Camley and D. L. Mills, "Theory of microwave propagation in dielectric/magnetic film multilayer structures," J. Appl. Phys., vol. 82, pp. 3058-67, 1997

[4]   N. Cramer, D. Lucic, R. E. Camley, and Z. Celinski, "High attenuation tunable microwave notch filters utilizing ferromagnetic resonance," J. Appl. Phys., vol. 87, pp. 6911-3, 2000

[5]   V. S. Liau, T. Wong, W. Stacey, S. Ali, and E. Schloemann, "Tunable band-stop filter based on epitaxial Fe film on GaAs," IEEE MTT-S, vol. 3, pp. 957-60, 1991

[6]   C. S. Tsai, Jun Su, and C. C. Lee, "Wideband electronically tunable microwave bandstop filters using iron film-gallium arsenide waveguide structure," IEEE Trans. Magn., vol. 35, pp. 3178-80, 1999

[7]   N. Cramer, D. Lucic, D. K. Walker, R. E. Camley and Z. Celinski, "Microwave tunable filters and phase-shifters based on transmission lines incorporating ferromagnetic metals," Submitted to IEEE Trans. Magn.

[8]   B. C. Wadell, Transmission Line Design Handbook, Boston: Artech House, 1991.

[9]   F. T. Ulaby, Fundamentals of Applied Electromagnetics, Upper Saddle River: Prentice Hall, 1999.

[10] R. J. Astalos and R. E. Camley, "Theory of a high frequency magnetic tunable filter and phase shifter," J. Appl. Phys., vol. 83, pp. 3744-9, 1998

[11] R. B. Marks and D. F. Williams, "A General Waveguide Circuit Theory," J. Res. NIST, vol. 5, pp. 533-62, 1992.

Incorporation of Ferromagnetic Metallic Films in Planar Transmission Lines for Microwave Device Applications

N. Cramer, *Student Member, IEEE*, D. Lucic, D. K. Walker, *Member, IEEE*, R. E. Camley, and
Z. Celinski, *Member, IEEE*

Abstract—We constructed a series of microstrip and co-planar microwave waveguides. These structures use metallic ferromagnets and therefore exhibit strongly frequency-dependent attenuation and phase-shift effects. The lines have maximum attenuation peaks occurring at the ferromagnetic resonance frequency, which increases with applied magnetic field. Such properties are used in band-stop filters. The devices used monocrystalline Fe films grown by Molecular Beam Epitaxy and polycrystalline sputtered permalloy films. For our devices that incorporated Fe the band-stop frequencies ranged from 10–20 GHz for applied fields up to only 80 kA/m (1000 Oersted). For devices using permalloy, the band-stop frequency was in the 5–10 GHz range for applied fields less than 80 kA/m. The maximum power attenuation was about 100 dB/cm, much larger than the previously reported values of 4 dB/cm. The resonance condition also affects the phase of the transmitted wave, strongly changing phase above and below the resonance frequency. The result is a phase-shifter that is tunable with applied magnetic field. We observed phase changes of over 360°/cm with an applied field of less than 40 kA/m.

Index Terms—Coplanar waveguide, ferromagnetic resonance, filter, microstrip, phase shifter.

Fig. 1. Schematic diagrams of (a) microstrip and (b) co-planar waveguide structures.

I. INTRODUCTION

MICROWAVE devices are widely used in both military and civilian communications systems. During recent decades, we have witnessed much progress in high-frequency semiconductor electronics and, in particular, the integration of different electronic components into circuits. An obvious obstacle to the increased use of microwave and millimeter-wave technology is the lack of advances in magnetic structures at high frequencies, for example, from 5–100 GHz.

Insulating ferrimagnetics such as YIG are well established in microwave applications [1]. These materials, however, have one significant drawback; their saturation magnetization, M_s, is low and therefore their operating frequency for moderate applied fields only covers a range of a few GHz. Here we report on the use of ferromagnetic metallic films in microwave transmission lines. These materials have higher M_s and thus have
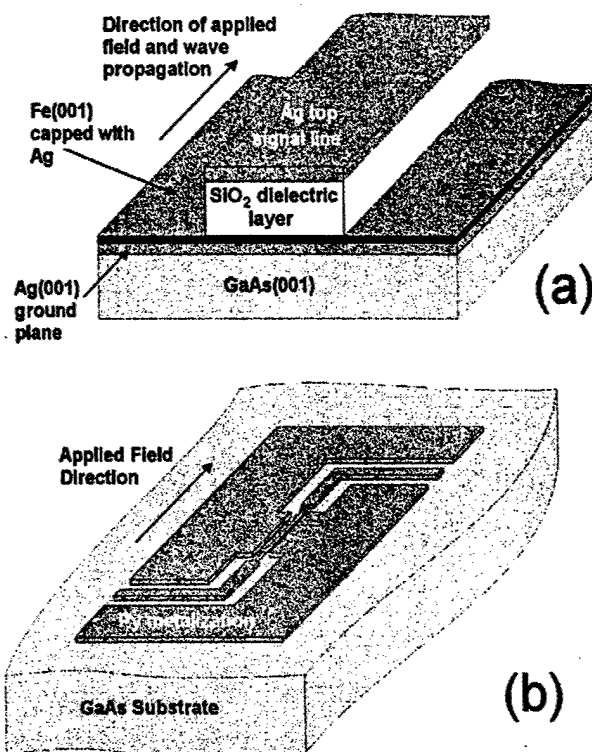
much higher operating frequencies. The theoretical treatment of such devices was explored by Schloemann and co-workers [2], Camley and Mills [3], and Huynen *et al.* [4].

We studied two types of transmission lines, microstrip and co-planar waveguide (CPW). For the microstrip, shown in Fig. 1(a), a ground plane of Ag(001) was grown on GaAs(001) by molecular beam epitaxy (MBE). This provided a template for a Fe(001) single-crystal film (200 nm), which was then capped with a thin Ag layer to prevent oxidization of the Fe [5], [6]. The sample was then transferred to an e-beam evaporation system for deposition of the dielectric layer and signal line. We deposited 4 μm of SiO_2 followed by 2 μm of Ag using a shadow mask to define the strip geometry. The width of our microstrip line ranged from 80 to 120 μm.

For the CPW structures, one of which is shown in Fig. 1(b), we again used GaAs substrates. However, in this case the sample

Fig. 2. Photograph of CPW line showing one right-angle bend and width transition.

Fig. 3. Tunable band-stop behavior of the Py-based CPW line.

was prepared in a sputtering system. We deposited a permalloy (Py) film 250 nm on top of a thin Ta adhesion layer. The Py was protected from oxidization with a thin Cu film. The films were patterned by photolithography followed by sputter etching in an Ar atmosphere. The lines were designed for a nominal characteristic impedance of 50 Ω. The waveguides made two right-angle bends to allow probes to contact from the sides, while a field was applied parallel with the length of the line. The lines are wide near the two ends to allow for probing but narrow in the middle to increase the magnitude of the resonance effects. Fig. 2 shows a photograph of one right-angle bend and width transition, including dimensions.

II. THEORY

In our devices, ferromagnetic resonance (FMR) produces absorption and phase-shift effects. The resonance occurs at a frequency given by

$$\omega = \gamma \sqrt{(H + H_a)(H + H_a + 4\pi M_S)} \qquad (1)$$

wher

H　　　is the applied magnetic field,

H_a　　defines the 4-fold anisotropy field in the direction of the applied field,

γ　　　is the gyromagnetic ratio, and

$4\pi M_s$　is the saturation magnetization.

Note that larger M_s values, such as those in Fe and Py, substantially increase the resonance frequency. For reference, the $4\pi M_s$ values for YIG, Py and Fe are 0.175 T, 1 T, and 2.15 T, respectively. Also, the anisotropy field, H_a, in single-crystal Fe is substantial—0.06 T, compared with nearly 0 for YIG and Py.

Consider the magnetic permeability of a ferromagnetic material in an applied field. As Schloemann proposed [2], the "Voigt permeability (μ_{voigt})," a complex scalar, accurately describes
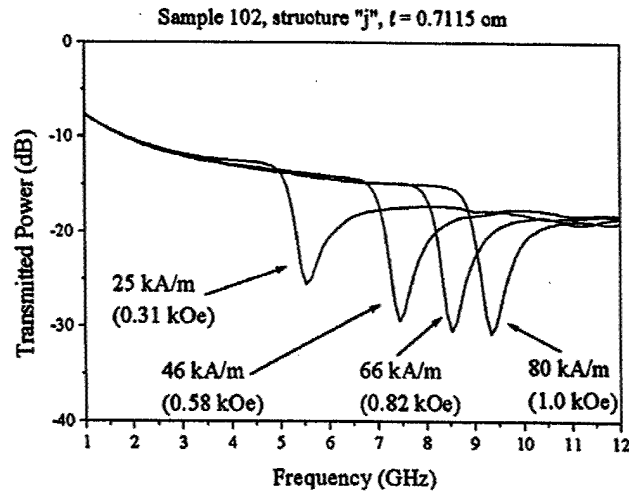
these effects. The relevance of this approach was rigorously confirmed later by Astalos and Camley [7]. At FMR, the imaginary part of μ_{voigt} becomes very large, leading to resonant absorption of microwave power. The real part of μ_{voigt} behaves like the real part of $\epsilon(\omega)$ near resonance, leading to a shift in the phase of a microwave signal.

III. RESULTS AND DISCUSSION

In a previous report [8], we demonstrated a band-stop filter implemented with Fe in a microstrip structure. This device showed large power attenuation at the band-stop frequency—over 100 dB/cm. The filter frequency was tunable over a range from 12–17 GHz by means of applied fields up to 40 kA/m. However, some performance limitations resulted due to our fabrication capabilities at that time. One problem was creating a 50 Ω line for impedance matching. The shadow mask we used to define the strip width created lines too wide for practical dielectric thicknesses, thus creating lines with a characteristic impedance much less than 50 Ω. Another limitation was the large resonance linewidth of our Fe films, which lead to broadening of the band-stop notch. Finally, the microstrip geometry is difficult to construct and to integrate with high-frequency electronics. In order to address these issues, we designed and constructed CPW transmission lines using Py as the magnetic component.

An example of the band-stop behavior of Py CPW lines is shown in Fig. 3. We observed power attenuation of about 20 dB/cm at the resonance frequencies, which were varied from 5–10 GHz with an applied field of up to 80 kA/m. The CPW lines were produced with characteristic impedances within 5 Ω of the desired value of 50 Ω. This is much better than obtained with the microstrip lines, and hence the power transmitted outside of the band-stop region was much higher. The background attenuation observed is due to reflection off the sharp corners and abrupt width change in the line—effects that can be minimized in a real device. The width of the stop band is under 1 GHz, compared with the nearly 3 GHz width observed in the Fe-based microstrip.
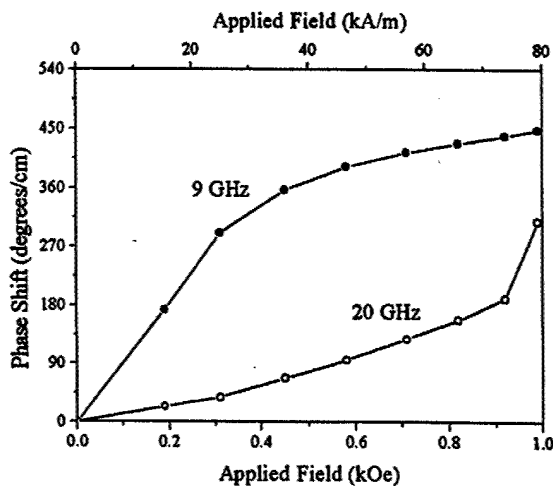
Fig. 4. Relative changes in phase of transmitted microwaves through a Fe-based microstrip verses applied magnetic field for two frequencies.
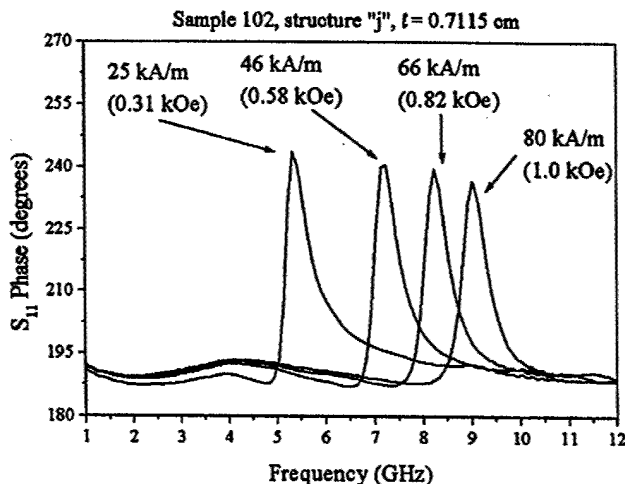

Fig. 5. Phase of reflected signal from a Py CPW line for various fields.

The Fe-based microstrip produced not only the band-stop effect, but also considerable tunable phase-shift effects. Fig. 4 shows the relative changes in phase shift as a function of applied field. For the frequencies of 9 and 20 GHz, we observed phase-shift tuning ranges of 450 and 270°/cm, respectively, as fields of up to 80 kA/m were applied. Note that these two frequencies lie below and above the tuning range of the stop band and therefore correspond to frequencies of low attenuation. For example, at 20 GHz, there is only about 6 dB/cm change in power attenuation over the range of applied field.

In the Py-based CPW lines, the phase-shift tuning of the transmitted signal (30°/cm) was much smaller than the effect observed in the Fe-based microstrip. This is due in large part to the narrower resonant absorption frequency width in Py, which substantially shifts phase only in regions of high attenuation of transmitted power. Fig. 5 shows a significant change in the

phase shift of a reflected signal. Furthermore, there was virtually no change in the magnitude of the reflected power at peak phase changes. In contrast to the continuously-variable phase shift possible in the Fe-based microstrip, the Py structure exhibited abrupt phase shift changes of over 50°. In addition, the magnitude of the effect in the Py structures showed no length dependence, suggesting that such a device could be reduced considerably in size.

IV. CONCLUSIONS

We developed tunable band-stop filters and phase-shifters based on two different ferromagnetic metals, Fe and Py, in microstrip and CPW. For Fe-based microstrip lines, we observed substantial attenuation of over 100 dB/cm and continuously variable phase-shift of over 360°/cm with applied fields of less than 40 kA/m. This attenuation is much higher than previously-reported values of 4 dB/cm [9], [10]. For Py-based CPW devices, we observed attenuation of 20 dB/cm. Changes in transmitted phase-shift are small. However, there are significant phase-shift changes in the reflected signal. These results demonstrate that use of ferromagnetic metallic films in transmission-line structures may have practical application in future microwave devices.

ACKNOWLEDGMENT

REFERENCES

[1] W. S. Ishak, "Magnetostatic wave technology: A review," *Proc. IEEE*, vol. 72, pp. 171–187, 1988.
[2] E. Schloemann, R. Tustison, J. Weissman, H. J. Van Hook, and T. Varitimos, "Epitaxial Fe films on GaAs for hybrid semiconductor-magnetic memories," *J. Appl. Phys.*, vol. 63, pp. 3140–3142, 1988.
[3] R. E. Camley and D. L. Mills, "Theory of microwave propagation in dielectric/magnetic film multilayer structures," *J. Appl. Phys.*, vol. 82, pp. 3058–3067, 1997.
[4] I. Huynen, G. Goglio, D. Vanhoenacker, and A. Vander Vorst, "A novel nonstructured microstrip device for tunable stopband filtering applications at microwaves," *IEEE Microwave Guided Wave Lett.*, vol. 9, pp. 401–403, 1999.
[5] G. A. Prinz and J. J. Krebs, "Molecular beam epitaxial growth of single-crystal Fe films on GaAs," *Appl. Phys. Lett.*, vol. 39, pp. 397–399, 1981.
[6] Z. Celinski, K. B. Urquhart, and B. Heinrich, "Using ferromagnetic resonance to measure magnetic moments of ultrathin films," *J. Magn. Magn. Mater.*, vol. 166, pp. 6–26, 1997.
[7] R. J. Astalos and R. E. Camley, "Theory of a high frequency magnetic tunable filter and phase shifter," *J. Appl. Phys.*, vol. 83, pp. 3744–3749, 1998.
[8] N. Cramer, D. Lucic, R. E. Camley, and Z. Celinski, "High attenuation tunable microwave notch filters utilizing ferromagnetic resonance," *J. Appl. Phys.*, vol. 87, pp. 6911–6913, 2000.
[9] V. S. Liau, T. Wong, W. Stacey, S. Ali, and E. Schloemann, "Tunable band-stop filter based on epitaxial Fe film on GaAs," *IEEE MTT-S*, vol. 3, pp. 957–960, 1991.
[10] C. S. Tsai, J. Su, and C. C. Lee, "Wideband electronically tunable microwave bandstop filters using iron film-gallium arsenide waveguide structure," *IEEE Trans. Magn.*, vol. 35, pp. 3178–3180, 1999.

High attenuation tunable microwave notch filters utilizing ferromagnetic resonance

N. Cramer, D. Lucic, R. E. Camley, and Z. Celinski[a]
Department of Physics, University of Colorado at Colorado Springs, Colorado Springs, Colorado 80933-7150

We have constructed a series of microstrips for transmission of microwaves. These microstrips incorporate ferromagnetic and dielectric layers and therefore absorb microwave energy at the ferromagnetic resonance (FMR) frequency. The absorption notch in transmission can be tuned to various frequencies by varying an external applied magnetic field. For our devices, which incorporate Fe as the ferromagnetic material, the resultant FMR frequencies range from 10–20 GHz for applied fields up to only 1000 Oe. This frequency range is substantially higher than those found in devices utilizing a dielectric ferrimagnet such as YIG. We constructed devices using monocrystalline Fe films grown in a molecular beam epitaxy system. Our devices are of different construction than other Fe dielectric microstrips and show much improvement in terms of notch width and depth. We observed maximum attenuation on the order of 100 dB/cm, much larger than previously reported values of 4 dB/cm. © *2000 American Institute of Physics.*
[S0021-8979(00)70308-2]

INTRODUCTION

Tunable filters based on the ferrimagnetic dielectric YIG are a well-established technology with many practical applications.[1] Band-stop filters, for example, rely on ferromagnetic resonance (FMR) to absorb microwave power at the FMR frequency. This frequency is set by material properties, such as saturation magnetization, M_s, anisotropy fields, H_a, the gyromagnetic ratio, γ, and the magnitude of an applied field, H. If the applied field is along the easy axis, the frequency is given by

$$\omega = \gamma \sqrt{(H + H_a)(H + H_a + 4\pi M_s)},$$

and therefore the resonance frequency can be varied with an electromagnet. The maximum field produced by the electromagnet determines the upper limit for the band-stop frequency. Hence, high frequencies are difficult to achieve with a device of limited physical size.

An alternative that has received attention in recent years is the use of a high M_s material such as Fe. While Fe has a much higher resonance frequency for the same applied field, its conductivity can lead to high loss at microwave frequencies. However, structures utilizing thin Fe films minimize conduction loss while still producing high attenuation at the band-stop frequency.[2,3]

Recent attempts at producing Fe-film-based structures have succeeded in making filters with high band-stop frequencies and low broadband loss.[3,4] However, the maximum attenuation has only reached about 4–5 dB/cm. We constructed microstrip band-stop filters using a slightly different geometry and growth method, resulting in much higher attenuation.

[a]Electronic mail: zcelinsk@mail.uccs.edu

EXPERIMENT

Previous filter structures used Fe epitaxial films grown directly on semi-insulating GaAs wafers. The backside of the wafer and the Fe films were then coated with a high-conductivity metal. The Fe side was then etched into a strip to form the microstrip structure shown in Fig. 1(a). For these filters, high quality, epitaxial Fe[5,6] (linewidth of ~35 Oe) is required to get reasonable attenuation.

Our devices, in contrast, consist of layers deposited on only one side of a GaAs(001) wafer as shown in Fig. 1(b). This allows us to have a much thinner dielectric layer which ultimately results in a much higher attenuation. The first stage of film growth was performed with molecular beam epitaxy (MBE) at a pressure of $\sim 10^{-9}$ Torr during deposition. Deposition was monitored both with a quartz thickness monitor and with reflection high-energy electron diffraction (RHEED).
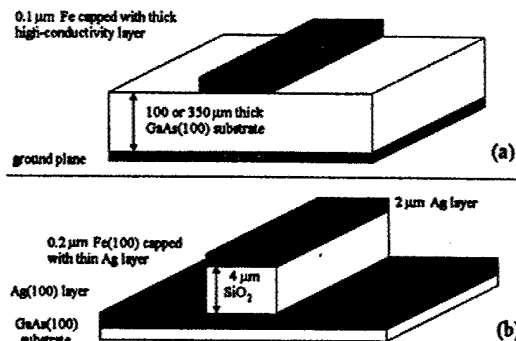

FIG. 1. Perspective cross sections for Scholemann structure using a GaAs(100) wafer as the dielectric layer (a). Our structure (b) is formed with vacuum-deposited SiO_2 as the dielectric. Note that the dielectric in (b) only exists directly below the microstrip, allowing single-sided probing.
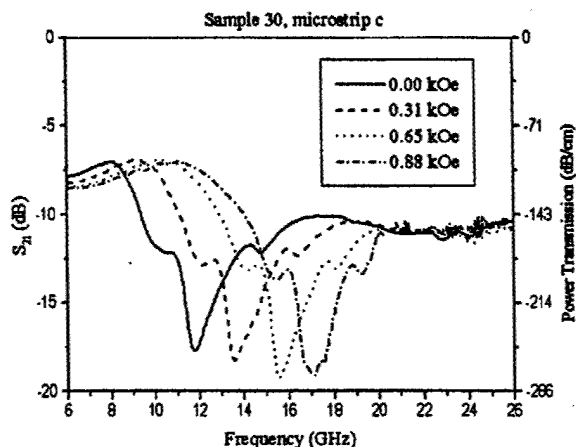
FIG. 2. Magnitude of S_{21} as a function of frequency. S_{21} represents voltage attenuation and therefore power attenuation is double in terms of dB.
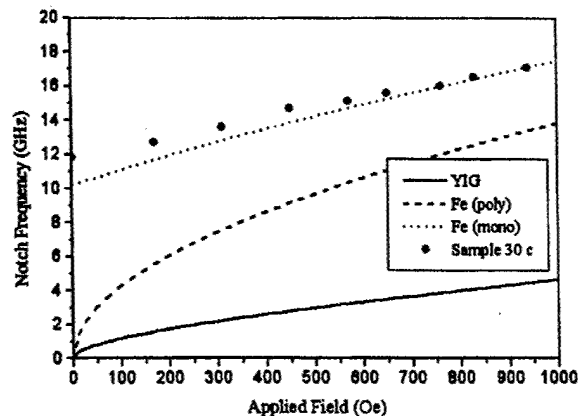

FIG. 3. Stop-band center frequency as a function of applied magnetic field for various structures. The plot for monocrystalline Fe represents our structure with the microstrip aligned with an easy axis.

First, a 1 nm thick Fe(001) "seed" layer was grown on a GaAs(001) substrate. A 600 nm layer of Ag(001) was then deposited and annealed at 520 K. This Ag film provides a ground plane and the template for further growth of epitaxial Fe(001). Next, 200 nm of Fe(001) was added and then covered with 5 nm of Ag to protect it from oxidation. Fe film quality was measured with FMR. This also allowed us to determine the easy axis of the film. Creating microstrips aligned with the easy axis increased the effective field in the strip and increased the operating frequency.

The sample was then transferred to a traditional e-beam evaporation system to complete the structure. A shadow mask was clipped on top of the sample before deposition to mask the ground plane and expose the microstrip shape. 4 μm of SiO_2 was deposited and capped with 2 μm Ag to form the dielectric and upper conductor, respectively. Note that because the ground plane is exposed on either side of the microstrip, the strip can be probed from the top side of the wafer.

Magnetic anisotropy, saturation magnetization, and resonance linewidth were all measured in 10 and 24 GHz FMR systems. Filter properties were measured with a Hewlett Packard 40 GHz vector network analyzer. This system allowed measurement of reflection, transmission, and characteristic impedance.

RESULTS AND DISCUSSION

Our FMR measurements showed a fourfold in-plane anisotropy field of 550 Oe. The resonance linewidth was approximately 50 Oe at 10 GHz for the monocrystalline Fe sample.

The magnitude of the ratio of transmitted voltage to input voltage, S_{21}, as a function of frequency is shown in Fig. 2 for our 0.14 cm long microstrip. The separate data sets represent applied fields ranging from 0 to 880 Oe. The stop-band depth is about 10 dB voltage attenuation or 20 dB power attenuation. For our short sample, this results in a

power attenuation of over 100 dB/cm. The tremendous increase in attenuation at the stop-band center frequency compared to earlier devices is due to the use of the thinner dielectric as predicted by theory.[7]

The observed insertion loss of about 7 dB is primarily due to impedance mismatch. This could be improved either by increasing the thickness of the dielectric or by narrowing the width of the upper conducting strip. Currently, we are restricted to a maximum dielectric thickness due to our probe station and we are restricted to a minimum strip width due to use of a shadow mask.

The variation in notch frequency with applied field follows theory reasonably well as shown in Fig. 3. By placing the strip along an easy axis, we create an effective field in the strip that is the sum of applied external field and anisotropy field. Thus, the effective field is boosted by 550 Oe. Figure 3 includes a theoretical plot for monocrystalline Fe with this anisotropy and also shows plots for polycrystalline Fe and YIG for comparison. Clearly, monocrystalline Fe produces much higher frequencies for similar fields than either of the other two.

CONCLUSION

We have created a band-stop filter with center frequencies in the 10–20 GHz range which is tunable with a small external magnetic field. This device represents two major improvements over other similar devices: (1) We find substantially higher attenuation in the stop band and (2) our structure obtains high attenuation even with higher Fe linewidths.

These improvements allow a great reduction in size for a complete device including an electromagnet. Raising the frequency range reduces the applied field required to create a high center frequency and thus reduces the electromagnet size. Increasing the attenuation reduces the microstrip length required and allows the electromagnet pole pieces to be placed closer together. This allows the same field strength to be created with a smaller magnet. In addition, our structure

should allow for integration with high-speed electronics on a single wafer.

ACKNOWLEDGMENTS

[1] W. S. Ishak, Proc. IEEE 76, 171 (1988).

[2] E. Schloemann, R. Tustison, J. Weissman, H. Jerrold Van Hook, and T. Varitimos, J. Appl. Phys. 63, 3140 (1988).

[3] V. S. Liau, T. Wong, W. Stacey, S. Ali, and E. Scholemann, IEEE MTT-S Dig. 957 (1991).

[4] C. S. Tsai, C. C. Lee, J. Su, W. So, W. Zuo, W. Wu, H. J. Yoo, G. Giergiel, H. Hopster, and D. L. Mills, Abstracts of Materials Research Society 1999 Spring Meeting, 5–9 April 1999, p. 169.

[5] G. A. Prinz and J. J. Krebs, Appl. Phys. Lett. 39, 397 (1981).

[6] Z. Celinski, K. B. Urquhart, and B. Heinrich, J. Magn. Magn. Mater. 166, 6 (1997).

[7] R. E. Camley and D. L. Mills, J. Appl. Phys. 82, 3058 (1997).

Dynamic and static measurements on epitaxial Fe/Si/Fe

Bijoy K. Kuanr[a)]
Department of Physics, University of Colorado at Colorado Springs, Colorado Springs, Colorado 80918

M. Buchmeier, D. E. Buergler, and P. Gruenberg
Forschungszentrum Juelich GmbH, Juelich, Germany

R. Camley and Z. Celinski
Department of Physics, University of Colorado at Colorado Springs, Colorado Springs, Colorado 80918

Strong antiferromagnetic interlayer exchange coupling across an insulating spacer is in increasing demand for high-density magnetic recording. We report here on the interlayer exchange coupling of epitaxial Fe(8 nm)/Si(t)/Fe(10 nm) trilayers as a function of Si thickness studied by ferromagnetic resonance (FMR), Brillouin light scattering, and magneto optic Kerr effect (MOKE) measurement techniques. A very strong antiferromagnetic (AFM) interlayer exchange coupling (>6 erg/cm^2) was observed at a spacer Si thickness of 0.7 nm. The bilinear J_1 and biquadratic J_2 coupling constants were determined from (i) the fitting of the angular variation of the resonance field (H_{res}) in FMR experiments, (ii) the field variation of the frequencies of the Damon–Eshbach surface modes (both optic and acoustic) in BLS measurements, and (iii) the fitting of longitudinal MOKE hysteresis loops. We obtain a higher H_{res} along the easy axis than along the hard axis and the magnetizations of the two Fe films are canted. The eightfold-like symmetry of H_{res} as a function of the angle observed at room temperature is due to the competition between the Fe fourfold anisotropy and AFM interfacial coupling energy. This behavior vanishes at low temperatures due to a strong increase of AFM coupling (especially J_2) in comparison to fourfold in-plane anisotropy. From the fitting of the temperature dependent FMR data, we obtain the temperature variation of the bilinear and biquadratic exchange coupling constants. We distinguish the existence of canted magnetization states at resonance by fitting the experimental H_{res} versus θ_H data to the model calculation. © *2003 American Vacuum Society.* [DOI: 10.1116/1.1562181]

I. INTRODUCTION

Studies of magnetic interactions between two ferromagnetic films separated by a nonmagnetic spacer have been a subject of extensive research for the past two decades. Elements like Cr, Cu, Ag, and Pd were extensively studied as spacers[1,2] to understand the nature and strength of interlayer exchange coupling. Typically the observed coupling strength was smaller than 1 erg/cm^2. For practical applications such as high density recording, a strong antiferromagnetic (AFM) exchange coupling across insulating spacer material is desirable. The Fe/Si exchange coupled multilayer system is a strong potential candidate due to its unusually high antiferromagnetic exchange coupling.[3-8] This coupling exhibits a strong exponential decay versus spacer thickness.[5,6] It was suggested before that in the Fe/Si/Fe system most of the Si had turned into metallic FeSi[5] due to Fe diffusion.

Ferromagnetic and antiferromagnetic exchange coupling in magnetic multilayers are frequently studied by two dynamical techniques—ferromagnetic resonance (FMR) and Brillouin light scattering (BLS).[1,2,9] The modes observed by FMR and BLS[9-11] (acoustic and optic branches) are sensitive to the magnetic energy within each ferromagnetic film as well as the interlayer exchange coupling across the nonmagnetic spacer. In addition, the magneto optic Kerr effect (MOKE) technique, which measures the static properties of

the material, is widely used to determine the strength of antiferromagnetic coupling between layers. To determine ferromagnetic coupling strengths by MOKE one has to turn to a spin engineering technique similar to one developed by Parkin.[12]

We have studied the bilinear (J_1) and biquadratic (J_2) exchange coupling of Fe/Si/Fe trilayers as a function of Si thickness and temperature. We use dynamic (FMR and BLS) and static (MOKE) techniques and the results obtained by the different techniques show good agreement. We find extremely strong antiferromagnetic coupling at a Si thickness of 0.7 nm for room temperature. The magnitude of the biquadratic coupling constant decreases very rapidly as the temperature increases.

II. EXPERIMENTS

Epitaxial Fe/Si/Fe trilayers, with Si thickness between 0.6 and 1.2 nm, were grown by molecular beam epitaxy (MBE) on a GaAs(100)/Fe(1 nm)/Ag(150 nm) substrate-buffer system. The background pressure was better than 10^{-9} mbar. The deposition rate was maintained at 0.1 Å/s for both Fe and Si. During the depositions of Fe and Si, the substrate was kept at room temperature. The thickness and deposition rate were controlled by a calibrated quartz-crystal monitor. The samples were characterized *in situ* by Auger electron spectroscopy (AES), low energy electron diffraction (LEED), and reflection high-energy electron diffraction (RHEED). Both
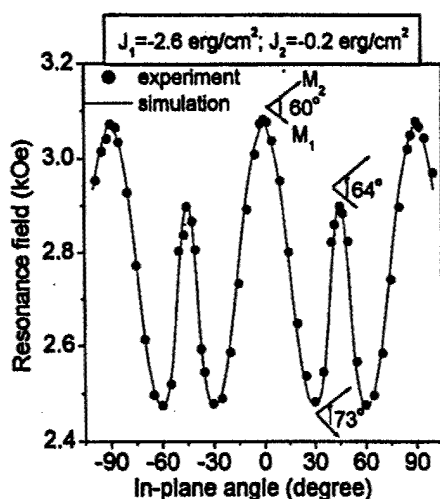
[a)]Electronic mail: bkuanr@brain.uccs.edu

FIG. 1. In-plane angular (θ_H) variation of acoustic resonance field (H_{res}) at room temperature (experimental; ● and theoretical;—) for antiferromagnetically coupled Fe(8 nm)/Si(1.0 nm)/Fe(10 nm) trilayer film studied by FMR at 24 GHz. The insets show the Fe magnetization directions at different resonance field values.

RHEED and LEED indicated epitaxial growth of Fe and Si layers. The samples were covered with a 50 nm ZnS antireflection layer that also prevents oxidation of the top Fe layer.

The magnetic properties of the exchange coupled samples were characterized through the study of resonance field modes (acoustic and optic) as a function of in-plane field angle with 24 and 35 GHz FMR spectrometers. A closed cycle helium Dewar was used to cool the sample from room temperature down to 25 K. The BLS experiments were performed at room temperature, in the backscattering geometry, with a (2×3) pass tandem Fabry–Perot interferometer.[1,9] The inelastically scattered light, corresponding to both the Stoke and the anti-Stoke, was recorded using an avalanche diode and a multichannel analyzer PC card. The free spectral range of the interferometer was ± 50 GHz. The wavelength $\lambda = 532$ nm of the incident laser light together with an angle of incidence of 45° resulted in an in-plane magnon wave vector $k_{\parallel} = 1.65(10^7)$ m^{-1}. A variable external field with a maximum strength of 7 kOe was applied in the sample plane and normal to the magnon wave vector. The surface modes of acoustic and optic spin waves were recorded on both the Stokes and the anti-Stokes sides of the spectrum. In addition, we used longitudinal MOKE measurements to record the hysteresis curves of the samples at room temperature.

III. RESULTS AND DISCUSSION

Figure 1 shows the in-plane angular variation of the resonance fields for the acoustic modes, $H_{res}(\theta_H)$ for a Fe(8 nm)/Si(1 nm)/Fe(10 nm) sample, measured at 24 GHz and at room temperature. The dots are experimental data and the solid lines are the results of theoretical calculations for the resonance field positions.[9–11] The eightfold-like symmetry for $H_{res}(\theta_H)$ (four peaks from $-90°$ to $+90°$) is clearly apparent at room temperature. Surprisingly, we observed a

higher H_{res} along the direction which is normally the Fe easy axis (0, $\pm 90°$) than along the direction which is normally the hard axis ($\pm 45°$).

To interpret these data we used a rather complex dispersion relation calculated for a strongly AFM coupled trilayer with the field applied in the sample plane.[13] The equilibrium position of the magnetization vector was obtained for each applied field from the total free energy[9,11,13] (Zeeman, demagnetizing, cubic anisotropy, and exchange coupling energy) expression. Our energy minimization process[9,10] can be used for any AFM exchange coupling strength and for any magnetic state[13] (saturated or unsaturated) of the sample to obtain the resonance field positions. The solid line in Fig. 1 shows the results of this calculation. The coupling constants obtained from the best fit to the experimental data are $J_1 = -2.6$ erg/cm^2 and $J_2 = -0.2$ erg/cm^2. The values of the cubic anisotropy and magnetization obtained from the fit are close to room temperature bulk values.

The acoustic resonance seen in Fig. 1 occurs at an unsaturated state, i.e., the magnetizations in the individual films do not point in the direction of the external static field, but are canted. The canting angle (angle between M_1 and M_2) obtained from the simulation is 60° when the applied field is along the easy axis ($\theta_H = 0°$), increases to 73° when $\theta_H = 28°$ (near the minimum for H_{res},) and then decreases to 64° for the applied field along the (usual) hard axis ($\theta_H = 45°$). The insets to Fig. 1 show the direction of Fe magnetization vectors M_1 and M_2.

The observed eightfold-like symmetry is due to the strong competition between the fourfold anisotropy energy of Fe and the strong antiferromagnetic coupling energy due to the Si spacer. It is easy to immediately conclude that the AFM coupling energy is stronger than the cubic energy because $H_{res}(0°) > H_{res}(45°)$.

Normally it is necessary to have measurements on both the acoustic and optic modes in order to obtain J_1 and J_2. Due to magnetic field limitations we were not able to measure the optic resonance. Nonetheless, the excellent agreement of the experimental $H_{res}(\theta_H)$ data with the model calculation[10,11,13] demonstrates that it is possible to obtain the coupling constants J_1 and J_2 from the angular variation of acoustic resonance without the optic resonance because the Fe magnetizations in the trilayer are in a canted state.

Figure 2 shows $H_{res}(\theta_H)$ data for the same sample measured at room temperature with the 35 GHz FMR system. For the fields used in this experiment (4.8 to 6 kOe) both M_1 and M_2 are aligned along the applied magnetic field (shown in the inset to this figure) and one measures the normal acoustic resonance. Therefore the eightfold-like symmetry observed at 24 GHz vanishes at this frequency. Figure 2 shows a standard fourfold symmetry expected for (100) Fe, with the easy-magnetization axis along 0° and hard along 45°, and with zero uniaxial anisotropy. The solid line to the figure was obtained from the model calculation[10,11,13] using a g factor of 2.08, which yields the following magnetic parameters; $H_K = 0.55$ kOe and $4\pi M_S = 21$ kOe, in agreement with 24 GHz FMR results. Also, at this frequency we were not
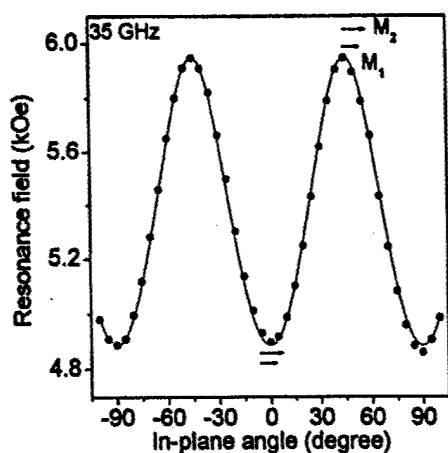
FIG. 2. FMR $H_{res}(\theta_H)$ data obtained from a 35 GHz FMR system [experimental (●) and theoretical (—)] for the Fe(8 nm)/Si(1.0 nm)/Fe(10 nm) trilayer.

FIG. 4. Acoustic resonance field (H_{res}) vs in-plane angle (θ_H) (experimental; ● and theoretical;—) for Fe(8 nm)/Si(1.0 nm)/Fe(10 nm) trilayer at 25 K.

able to measure the optic resonance due to the unavailability of a strong magnetic field.

Figure 3 shows the deduced coupling coefficients J_1 and J_2 as a function of Si spacer thickness (t) for Fe(8 nm)/Si(t)/Fe(10 nm) trilayers. The coefficients were obtained from room temperature FMR measurements at 24 GHz. We observed antiferromagnetic (AFM) exchange coupling for all studied thicknesses of Si spacers. The exchange coupling constants were derived from our $H_{res}(\theta_H)$ data. At a spacer thickness of 0.6 nm, the coupling is dominantly biquadratic; with $J_1 = -3.4$ erg/cm^2 and $J_2 = -2.65$ erg/cm^2, which is among the strongest biquadratic coupling ever found. The AFM coupling strength attained a maximum at 0.7 nm spacer thickness with $J_1 = -6.5$ erg/cm^2 and $J_2 = -1.1$ erg/cm^2. Both J_1 and J_2 decrease rapidly in magnitude for larger Si thicknesses (1.0 and 1.2 nm). It was observed that J_2 remains consistently smaller (in magnitude) than J_1 and decays faster. The strong decrease of bilinear coupling at smaller Si thickness could be explained in terms
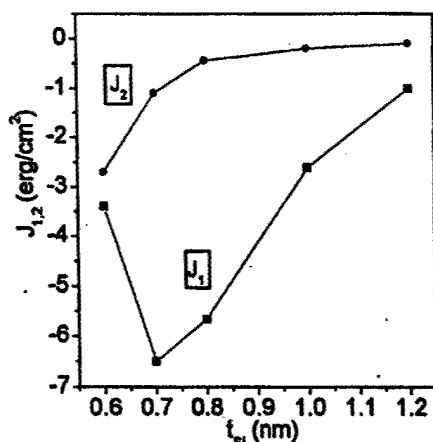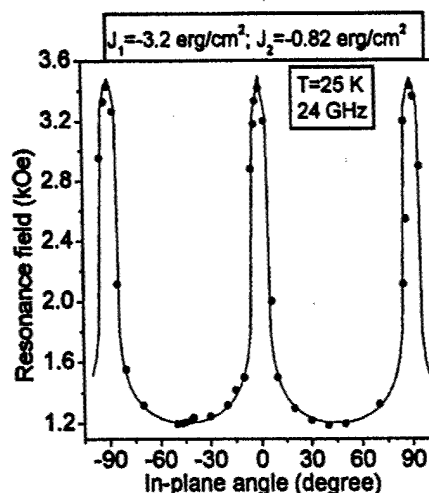
of Slonczewski's[14] theory by a competition of ferromagnetic (FM) (possibly due to pinholes) coupling and antiferromagnetic (AFM) interlayer coupling. The fast decay of J_2 with increasing spacer thickness is in agreement with this mechanism,[14] for example, because the number of pinholes decreases with increasing thickness of the Si spacer. The observed weak biquadratic coupling for Si thickness above 0.8 nm is in agreement with smooth decay of J_1, as predicted by Slonczewski.[14]

Figure 4 shows the $H_{res}(\theta_H)$ data for the same trilayer sample at 25 K. The figure depicts a fourfold symmetry, but with a higher H_{res} along the easy axis (0°) compared to that along the hard axis (45°). The coupling constants derived from the resonance fit[10,11,13] are $J_1 = -3.2$ erg/cm^2 and $J_2 = -0.82$ erg/cm^2 along with a small increase of the effective anisotropy field value (0.67 kOe). At 25 K, the resonance was observed at a canted state. However, the AFM coupling energy completely dominates the cubic anisotropy energy and therefore the eightfold-like symmetry, observed at room temperature, vanished at this low temperature.

Figure 5 compiles both J_1 and J_2 coupling constants for the Fe(8 nm)/Si(1.0 nm)/Fe(10 nm) trilayer sample from 25 to 300 K obtained from 24 GHz FMR measurements. We observed that both J_1 and J_2 decrease with increasing temperature (T). However, the temperature dependence of J_2 is much stronger than that of J_1. The biquadratic coupling increases fourfold from room temperature down to 25 K, whereas the bilinear coupling increases only slightly by a factor of 1.25 at 25 K to its value at room temperature.

The slow decrease of J_1 with temperature could be associated with reduced magnetization of Fe. For example, the magnetization and the linear exchange coupling constant, J_1, both saturate below 100 K. The temperature dependence of J_1 for insulating and metallic spacers can be described by the quantum interference model of Bruno.[16] We discuss our results in the light of available theories.[14-16] According to Slonczewski,[15] the increase of J_1 and J_2 can be mediated by

FIG. 3. Room temperature coupling strength of bilinear (J_1) and biquadratic (J_2) constants as a function of Si spacer thickness.
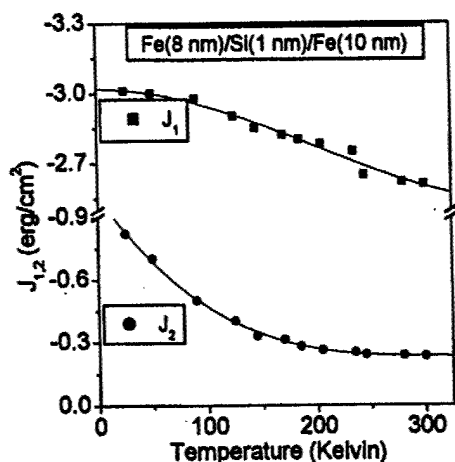
FIG. 5. Temperature dependence (25–300 K) of bilinear (J_1) and biquadratic (J_2) coupling strengths for Fe(8 nm)/Si(1.0 nm)/Fe(102 nm) trilayer film. The solid lines serve as a guide to the eye only.

loose spins present inside the spacer or adjacent to the Fe/Si interface, which can couple to both Fe layers via indirect exchange. Another possibility[14] resulting in a strong decrease of J_2 with temperature can be due to thickness fluctuations of the Si spacer. This causes a competition between FM and AFM coupling for neighboring regions, which may lead to a frustration of coupling. Strijkers et al.[6] favored the loose spin model[15] to interpret their data of strong exponential decay of J_2. On the contrary, Fullerton et al.[3] discussed their strong temperature dependence of biquadratic coupling data by spatial or compositional fluctuations at interfaces termed as a fluctuation mechanism by Slonczewski.[14] For all known biquadratic coupling mechanism, loose spin models,[15] the fluctuation model[14] and the intrinsic higher order term[16]–J_2 increases monotonically upon cooling.

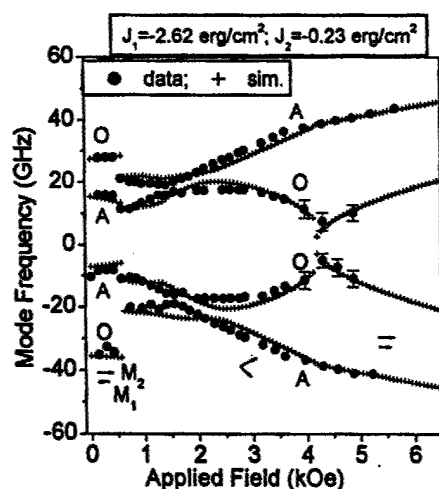In Fig. 6 we show the magnetic field dependence of BLS

FIG. 6. BLS mode frequencies vs magnetic field for the Fe(8 nm)/Si(1.0 nm)/Fe(10 nm) trilayer showing the acoustic (marked A) and optic (marked O) branches on both Stokes and anti-Stokes sides. The plus signs (+) are the theoretical calculation.

mode frequencies for the Fe(8 nm)/Si(1 nm)/Fe(1 nm) trilayer film with the magnetic field applied along the easy axis of the film. The two modes shown here (closed circles) are the acoustic and optic surface modes.[1,9,11] In a typical BLS spectrum the acoustic mode is identified as the higher intensity mode and the optic mode as the lower intensity mode. The acoustic modes are marked as "A" and the optic modes as "O" in the figure. The evolution of the spectra with magnetic field corresponds to changes in magnetization directions of M_1 and M_2. As the applied field is increased from zero, the two magnetizations change from an antiparallel configuration to a spin flop or canted state, and finally at high field to parallel alignment.

For the antiparallel alignment, the frequency of the optic mode is higher than that of the acoustic mode. A strong asymmetry of the Stoke and the anti-Stoke spectra reflects strong AFM coupling with antiparallel alignment of Fe magnetizations. The asymmetry and the sudden jump of mode frequencies reflect the transition of magnetization alignment from antiparallel to spin flop at 0.6 kOe and then from spin flop to parallel at 4.2 kOe magnetic field. In the spin flop region, the rotation of magnetizations towards field direction is accompanied by a crossing of the spin wave modes. From the theoretical simulations it is identified that the crossing point of the spin wave modes corresponds to an exact 90° alignment between M_1 and M_2.

At large applied fields M_1 and M_2 become parallel. In this case the difference in frequency between the acoustic and optic modes is a measure of the exchange coupling energy between the two ferromagnetic layers. We fitted the experimental results to the model calculation[9–11] to obtain the exchange coupling strengths J_1 and J_2. The quantitative evaluation of coupling constants is done by considering the equation of motion and boundary conditions.[9–11] The plus sign (+) indicating the results of the theoretical calculations were generated from a Levenberg–Marquardt fit to the experimental data. The strength of J_1 and J_2 obtained from the BLS data are −2.62 and −0.23 erg/cm², respectively. The BLS results and the FMR results are in good agreement for all the other samples with different Si thicknesses.

The BLS and FMR measurements above probe the dynamical properties of the samples. It is important to know if the static properties can be explained using the same parameters that apply to the dynamical system. We used MOKE to study the static magnetization as a function of applied field. The experimental easy and hard axis MOKE hysteresis loops are fitted[11] by considering the anisotropy (K_1), bilinear (J_1), biquadratic (J_2), and Zeeman energies. The hysteresis loops are simulated by minimizing the total free energy of the system with respect to the magnetization directions of the two Fe layers for each value of H. We can obtain both J_1 and J_2 coupling constants due to the existence of two plateaus in the hysteresis loops and the determined values are within 5% of the FMR and BLS results.

IV. CONCLUSION

We investigated Fe/Si/Fe trilayers with strong antiferromagnetic exchange coupling by FMR and BLS. Both tech-

niques provide the possibility to determine the bilinear (J_1) and biquadratic (J_2) coupling constants. The $H_{res}(\theta_H)$ curves were well understood from a theoretical calculation suited for strong AFM coupling. The observed eightfold-like symmetry is due to competition between strong AFM coupling energy and cubic anisotropy energy and results in an unusual situation where H_{res} is higher along the (normally) easy-axis direction compared to that along the hard axis. This behavior vanished at low temperature where AFM coupling energy completely dominates the anisotropy energy. At room temperature we obtain $J_1 = -2.6\,\text{erg/cm}^2$ and $J_2 = -0.2\,\text{erg/cm}^2$. These results are in excellent agreement with those obtained from fitting the mode frequencies in BLS experiments. We also find the behavior of J_1 and J_2 as a function of temperature and show that the magnitude of J_2 decreases rapidly as the temperature increases.

ACKNOWLEDGMENTS

[1] P. Gruenberg, R. Schreiber, Y. Pang, M. B. Brodsky, and H. Sower, Phys. Rev. Lett. **57**, 2442 (1986).

[2] B. Heinrich and J. A. C. Bland, *Ultrathin Magnetic Structures, I, II* (Springer, Berlin, 1994).

[3] E. E. Fullerton, J. E. Mattson, S. R. Lee, C. H. Sowers, Y. Y. Huang, G. Felcher, S. D. Bader, and F. T. Parker, J. Magn. Magn. Mater. **117**, L301 (1992); Phys. Rev. B **53**, 5112 (1996).

[4] A. Chaiken, R. P. Michel, and M. A. Wall, Phys. Rev. B **53**, 5518 (1996).

[5] J. J. de Vries, J. Kohlhepp, F. J. A. den Broeder, R. Coehoorn, R. Jungblut, A. Reinders, and W. J. M. de Jonge, Phys. Rev. Lett. **78**, 3023 (1997).

[6] G. J. Strijkers, J. T. Kohlhepp, H. J. M. Swagten, and W. J. M. de Jonge, J. Appl. Phys. **87**, 5452 (2000); Phys. Rev. Lett. **84**, 1812 (2000).

[7] R. R. Gareev, D. E. Bürgler, M. Buchmeier, D. Olligs, R. Schreiber, and P. Grünberg, Phys. Rev. Lett. **87**, 157202 (2001).

[8] P. Gruenberg, D. E. Bürgler, D. Olligs, R. R. Gareev, M. Buchmeier, B. K. Kuanr, and R. Schreiber, J. Phys. D **35**, 2403 (2002).

[9] B. K. Kuanr, M. Buchmeier, D. E. Buergler, and P. Gruenberg, J. Appl. Phys. **91**, 7209 (2002).

[10] M. Buchmeier, B. K. Kuanr, R. R. Gareev, D. E. Buergler, and P. Gruenberg (unpublished).

[11] S. M. Rezende, C. Chesman, M. A. Lucena, A. Azevedo, F. M. de Aguiar, and S. S. P. Parkin, J. Appl. Phys. **84**, 958 (1998).

[12] S. S. P. Parkin and D. Mauri, Phys. Rev. B **44**, 7131 (1991).

[13] J. Geshev, L. G. Pereira, and J. E. Schmidt, Physica B **320**, 169 (2002).

[14] J. C. Slonczewski, Phys. Rev. Lett. **67**, 3172 (1991).

[15] J. C. Slonczewski, J. Appl. Phys. **73**, 5957 (1993).

[16] P. Bruno, Phys. Rev. B **52**, 411 (1995).

Variation of magnetization and the Landé g factor with thickness in Ni–Fe films

J. P. Nibarger,[a] R. Lopusnik, Z. Celinski,[b] and T. J. Silva
National Institute of Standards and Technology, Boulder, Colorado 80305

We have measured the Landé g factor, the effective magnetization M_{eff}, the uniaxial anisotropy H_k, and the Gilbert damping parameter α, as a function of Permalloy film thickness from 2.5 to 50 nm. We used a pulsed inductive microwave magnetometer capable of generating dc bias fields of 35.2 kA/m (440 Oe). A significant decrease in g is observed with decreasing thickness below 10 nm. Also, M_{eff} decreases with decreasing thickness consistent with a surface anisotropy constant of 0.196 ± 0.025 mJ/m^2. The decrease in g can arise from the orbital motion of the electrons at the interface not being quenched by the crystal field. We also compare our data to a model of an effective g factor suggesting that the decrease in g factor might also stem from the Ni–Fe interface with a Ta underlayer. [DOI: 10.1063/1.1588734]

As the magnetic-data-storage industry develops disk drives with data transfer rates approaching 1 Gbit/s, understanding the underlying dynamics of the soft magnetic components used in recording heads becomes increasingly important. Two important material parameters that govern the response and precessional frequency of a magnetic film are the effective magnetization M_{eff} and the Landé g factor. M_{eff} affects the dynamics by generating internal demagnetizing fields during the switching process that greatly accelerate the precessional motion. The Landé g factor sets the proportionality of angular momentum and magnetic moment for the individual spins that results in precessional motion. For state-of-the-art heads with exceedingly small magnetic layer thicknesses, interfaces play a large role, and understanding the effect of interfaces on M_{eff} and g is crucial for the engineering of high-performance recording systems. The thickness dependence of M_{eff} and g in the case of thin Permalloy films was first measured by ferromagnetic resonance.[1]

We demonstrate the ability of a pulsed inductive microwave magnetometer (PIMM) to measure simultaneously the effective magnetization M_{eff}, the uniaxial anisotropy H_k, and the spectroscopic Landé g factor, at high dc bias fields. This is done for a thickness series of Permalloy films ($Ni_{81}Fe_{19}$) ranging from 2.5 to 50 nm. By applying large dc fields [35.2 kA/m (440 Oe)] along the easy axis of the sample during measurements, we are able to extract M_{eff}, g, and H_k simultaneously using a nonlinear, three-parameter fit. This is in contrast to most permeameters, which require a separate measurement of M_{eff}. In addition, the Gilbert damping parameter α, was extracted as a function of thickness.

Polycrystalline Permalloy films were deposited on 1 cm$\times$1 cm$\times$100 μm (0001) oriented sapphire coupons. The sapphire substrates were cleaned using ion milling in Ar/O$_2$ and Ar atmospheres to remove contaminants. Then, a dc magnetron operating in an Ar atmosphere at 0.533 Pa (4 mTorr) was used to sputter a 5 nm Ta adhesion layer. Permalloy films of 2.5, 5, 7.5, 10, 15, 25, or 50 nm thicknesses

were then deposited followed by a 5 nm capping layer of Cu to protect the Permalloy against oxidation. Samples were grown in a 20 kA/m (250 Oe) external magnetic field to induce uniaxial anisotropy. Photolithography and a nitric acid etch was used to pattern a 3 mm$\times$3 mm square in the center of the Permalloy coupon. The reduced sample area was required to guarantee high uniformity of the dc bias field across the area of the sample during measurements. Figure 1 upper inset shows typical hard- and easy-axis hysteresis loops of the unpatterned 50-nm-thick sample characterized using an induction-field looper to verify their quality.

Samples were measured by use of a PIMM.[2] A coplanar waveguide of 50 Ω impedance and 100 μm center conductor was used. The easy axis of the sample was aligned parallel to the center conductor, as shown in the lower inset of Fig. 1. A commercial pulse generator provided 10 V pulses, with 50 ps
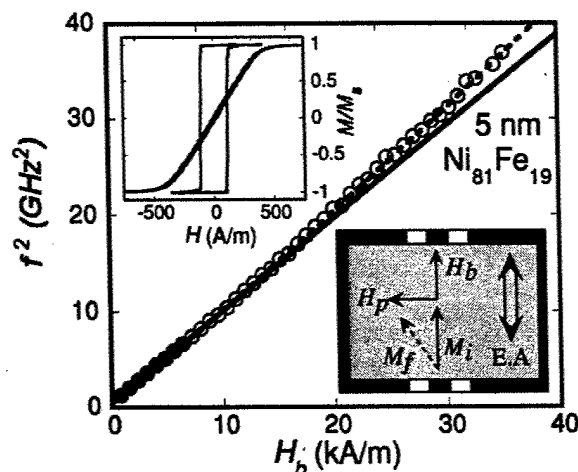

FIG. 1. Frequency squared as a function of bias field for a 5 nm sample; the error bars are the size of the circles. Data for bias field 0.8–7.16 kA/m (10–90 Oe) are shown with filled-in circles and fitted linearly with a solid line to demonstrate the deviation from linearity of the data at high bias fields. All of the data were fitted with Eq. (1) (dashed line). Lower inset shows the measurement geometry used for pulsed inductive microwave magnetometer measurements, with the easy axis of the sample parallel to the applied dc bias field. Upper inset shows induction field looper measurements of the unpatterned 50 nm thick sample showing the easy- and hard-axis hysteresis loops with easy-axis squareness of 0.99.

---

[a]Electronic mail: nibarger@boulder.nist.gov
[b]Present address: Department of Physics, University of Colorado at Colorado Springs, Colorado Springs, CO 80918.

rise times and 10 ns durations. The pulsed field H_p, was oriented along the hard axis of the sample. The nominal field pulse amplitudes were found by the use of the Karlquist equation for fields from a current strip[3] to be 800 A/m (10 Oe). The Permalloy films were placed facing the waveguide. To prevent shorting of the coplanar waveguide a thin layer of photoresist ($<1~\mu$m) was spin coated onto the sample.

Static longitudinal bias fields (H_b in Fig. 1 lower inset), ranging from 0.8 to 35.2 kA/m (10 to 440 Oe), were generated by an electromagnet with soft iron pole pieces and a circular yoke.[4] Field calibration was performed to avoid any effects of remanence and allowed the fields to be set with an uncertainty of 1%. Field uniformity along the waveguide was better than 1% over a length of 4 mm. Coil resistance was monitored to determine if any heating had occurred that could lead to field drift. If the resistance was more than 2.5% above room-temperature resistance, then data acquisition was temporarily stopped until the coils cooled.

Precessional response was measured with a 20 GHz-bandwidth digital sampling oscilloscope. The measured precession frequencies ranged from 1 to 6.5 GHz and were well within the bandwidth of the detection system.[2] A background response was obtained with an applied saturation field of 2.4 kA/m (30 Oe) along the hard axis and zero field along the easy axis. The precessional dynamics was extracted by subtracting the measured and background signals.

The induced voltage of the precessional response measured in the time domain was converted into frequency spectra by fast Fourier transform for further analysis. The Gilbert damping parameter α, was extracted from the full width at half maximum of the imaginary part of the spectrum $\Delta\omega$, such that: $\alpha \approx \Delta\omega/(\gamma\mu_0 M_{\text{eff}})$.[5] The resonance of the signal was extracted from the zero crossing of the real part of the spectrum. The resonance frequency as a function of bias field can be described by the Kittel formula for a thin film[6]

$$\omega_0^2 = \left(\frac{g\mu_B\mu_0}{\hbar}\right)^2 (M_{\text{eff}} + H_k + H_b)(H_k + H_b), \qquad (1)$$

where μ_B is the Bohr magneton, $\hbar$ is Planck's constant divided by 2π, and μ_0 is the permeability of free space. A simultaneous three-parameter fit of ω_0^2 vs H_b can be used to extract M_{eff}, g, and H_k. We emphasize that a three-parameter fit is possible only when a sufficiently large field range is used such that terms in Eq. (1) quadratic in bias field are no longer negligible. Fortunately, the applied dc fields need not be as large as M_{eff} for the nonlinearity in ω_0^2 vs H_b to be measurable. Since surface anisotropies may exist for very thin magnetic films, the demagnetizing fields induced by out-of-plane motion of the magnetization vector differs from the saturation magnetization by the usual surface anisotropy term[7]

$$\mu_0 M_{\text{eff}} = \mu_0 M_s - \frac{2K_s}{M_s \delta}, \qquad (2)$$

where δ is the film thickness and K_s is the average anisotropy, consisting of the sum of the Cu/NiFe and Ta/NiFe interface surface anisotropies.

Figure 1 is a plot of frequency squared, $f^2 = (\omega/2\pi)^2$ as a function of longitudinal bias field for a 5-nm-thick film. The uncertainty in f^2 is found to vary from 5% at 1 GHz^2 to
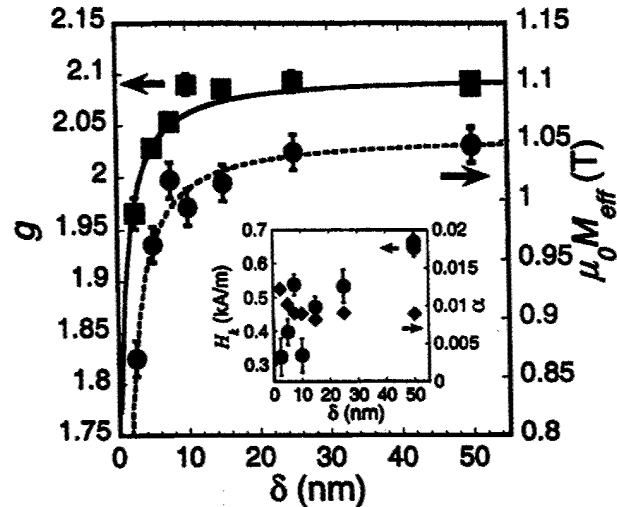

FIG. 2. $\mu_0 M_{\text{eff}}$ and g as a function of thickness, δ. Inset shows H_k and α as a function of δ. The α values plotted are with 8 kA/m longitudinal bias field applied. $\mu_0 M_{\text{eff}}$ was fitted to Eq. (2) (dashed line), yielding $\mu_0 M_s = 1.0553$ T and $K_s = 0.196$ mJ/m^2. The measured g factor is compared to Eq. (7) (solid line) where $T_{\text{Ta/NiFe}} = 0.6$ nm (see Ref. 12), $T_{\text{Cu/NiFe}} = 0.4$ nm, $g_{\text{NiFe}} = 2.1$ (see Refs. 1, and 13) $g_{\text{Ta/NiFe}} = 1.58$ (see Ref. 14), $g_{\text{Cu/NiFe}} = 2.05$ (see Ref. 15).

0.8% at 40 GHz^2.[2] The data can be fit using Eq. (1) (dashed line) to yield values of M_{eff}, g, and H_k. To highlight the deviation from linearity, data for 0.8–7.2 kA/m (10–90 Oe) bias fields (shown with filled-in circles) were fitted to a linear function of H_b, with the fit extrapolated to high fields. The data are as much as 8% greater than the linear extrapolation from low field data, showing the magnitude of the nonlinearity to be fitted in the extraction of M_{eff}, g, and H_k. For each thickness, multiple measurements were made to determine statistics for repeatability and to decrease noise through averaging. Due to the 1% uncertainty in bias fields, a systematic error of 2.5% for g, 4% for M_{eff}, and 12% error in H_k are presumed. Results for M_{eff} and g as a function of thickness δ, are shown in Fig. 2. H_k and α as a function of thickness is shown in Fig. 2 inset. The α values plotted are from data with an 8 kA/m longitudinal bias field.

The Gilbert damping parameter, α, increased with decreasing film thickness, consistent with previous measurements in Permalloy.[8] H_k appears to vary randomly with an average value of 408±40 A/m (5.1±0.5 Oe) for $2.5 < \delta < 15$ nm, with no observable trend within the error bars for the measurement. However, both M_{eff} and g decrease significantly with decreasing film thickness below 10–20 nm. In practical terms, the reduction in M_{eff} and g is a decrease in the intrinsic ferromagnetic resonance frequency for the thinnest Permalloy by 27% relative to the thickest films, equivalent to a shift in the precessional frequency of 230 MHz.

Values obtained for $\mu_0 M_{\text{eff}}$ with the PIMM are consistent with values obtained from an alternating gradient magnetometer (AGM). For 50 and 25 nm sample thicknesses the AGM measured values of $\mu_0 M_{\text{eff}}$ were 1.0630 and 1.0180 T, respectively, compared to 1.0462 and 1.0398 T, respectively, from the PIMM measurements. The observed decrease in $\mu_0 M_{\text{eff}}$ with decreasing thickness is consistent with a surface anisotropy contribution given by Eq. (2). A fit to Eq. (2) is shown in Fig. 2 as a dashed line. K_s is 0.196±0.025 mJ/m^2

and $\mu_0 M_s$ is 1.0553 ± 0.046 T. The error in K_s and $\mu_0 M_s$ accounts for both random error and the uncertainty of 1% for the bias field.

In general, both the orbital and spin angular momentum contribute to the total angular momentum of an electron. As such, the g factor may be written as

$$g = \frac{2m_e}{e} \frac{\mu_S + \mu_L}{\langle S \rangle + \langle L \rangle}, \qquad (3)$$

where μ_S and μ_L are the contributions to the electron magnetic moment due to the spin and orbital components, respectively. For a symmetric crystal lattice, the orbital motion of the electron during gyromagnetic precession is quenched by the crystal field, i.e., $\langle L \rangle = 0$. Thus, the orbital contribution to the electron angular momentum is zero even though the orbital contribution to the magnetic moment is nonzero resulting in a g factor that is always greater than two:[9]

$$g = \frac{2m_e}{e} \frac{\mu_S + \mu_L}{\langle S \rangle} = 2\left(1 + \frac{\mu_L}{\mu_S}\right). \qquad (4)$$

However, the orbital motion is not entirely quenched at surfaces and interfaces where the crystal field is no longer symmetric since the interface breaks inversion symmetry. Under such circumstances, the orbital motion can still contribute to the gyromagnetic motion. Equation (3) can then be written as

$$g = \frac{2m_e}{e} \frac{\mu_S}{\langle S \rangle} \frac{\left(1 + \frac{\mu_L}{\mu_S}\right)}{\left(1 + \frac{\langle L \rangle}{\langle S \rangle}\right)} \approx 2\left(1 - \frac{\mu_L}{\mu_S}\right), \qquad (5)$$

since $\langle S \rangle = \mu_S m_e/e$, $\langle L \rangle = 2\mu_L m_e/e$ and expanding the Taylor's series to first order. Thus, surfaces and interfaces allow for the possibility that the g factor is less than 2. Two physical mechanisms are plausible sources for this interface effect. First, the orbital motion is not quenched by the crystal field, i.e., $\langle L \rangle \neq 0$. In addition, material mixing at the interface could alter the g factor. We can model the later hypothesis of interface mixing by relying on the concept of an effective g factor, g_{eff}, first proposed by Wangness[10,11]

$$\frac{\rho_{\text{NiFe}} V_{\text{NiFe}} + \rho_{\text{Ta/NiFe}} V_{\text{Ta/NiFe}} + \rho_{\text{Cu/NiFe}} V_{\text{Cu/NiFe}}}{g_{\text{eff}}}$$

$$= \frac{\rho_{\text{NiFe}} V_{\text{NiFe}}}{g_{\text{NiFe}}} + \frac{\rho_{\text{Ta/NiFe}} V_{\text{Ta/NiFe}}}{g_{\text{Ta/NiFe}}} + \frac{\rho_{\text{Cu/NiFe}} V_{\text{Cu/NiFe}}}{g_{\text{Cu/NiFe}}}, \qquad (6)$$

where ρ_i, V_i, and g_i are the spin density, volume, and g factor for each of the respective layers or interfaces (i = NiFe, Ta/NiFe, Cu/NiFe). The volume V_i may be set equal to the thickness t_i since the interface area is the same for each layer. Equation (6) can be rewritten as a function of the thickness of the Permalloy film, δ:

$$g_{\text{eff}}(\delta) = \frac{\delta + t_{\text{Ta/NiFe}} + t_{\text{Cu/NiFe}}}{\dfrac{\delta}{g_{\text{NiFe}}} + \dfrac{t_{\text{Ta/NiFe}}}{g_{\text{Ta/NiFe}}} + \dfrac{t_{\text{Cu/NiFe}}}{g_{\text{Cu/NiFe}}}}. \qquad (7)$$

We assume that the spin density ρ_i is invariant through the film thickness and that reasonable assumptions for the Cu/NiFe and Ta/NiFe interface thickness and the g-factors for the films and interfaces can be made.

The mixing at Ta/NiFe interfaces has been well studied for magnetic random access memory (MRAM) and giant magnetoresistance applications. Kowalewski et al.[12] found the interface thickness for unannealed samples to be 0.6 nm. The thickness of the Cu/NiFe interfaces is approximately two monolayers (0.4 nm). The measured g factor for NiFe from this experiment for the thickest films is 2.1, which is consistent with other published values (2.08,[1] 2.08,[13] and 2.17).[13] For the g factor at the Ta/NiFe interface, we make a very coarse approximation and use the Ta bulk value of 1.58.[14] Likewise, the g factor for Cu/NiFe is simply that of bulk Cu, 2.05,[15] a value not too different from that of bulk Permalloy. A plot of Eq. (7) with the earlier assumption is shown in Fig. 2 with no adjustable parameters. The calculated reduction in g with decreasing NiFe thickness is in large part the result of the Ta interface, which has a large orbital contribution to the moment.

This model works surprisingly well as an explanation for the thickness variation of g, in spite of the particularly crude assumptions made of uniform spin density and bulk values for the g factors at the various interfaces. These two assumptions stem from the presumption that ferromagnetism persists even in an intermixed atomic environment, though the orbital momentum contribution to the total angular momentum of the ferromagnetic spins is dominated by the electronic structure of the nonmagnetic constituent. We conclude that either the orbital motion at the interface is not quenched by the crystal field, i.e., $\langle L \rangle \neq 0$, or that interfacial mixing of ferrous and nonferrous materials, or some combination of these two effects can explain the significant deviations of the precessional dynamics in thin Permalloy films from that predicted from bulk values of the g factor.

[1] M. H. Seavey and P. E. Tannenwald, J. Appl. Phys. **29**, 292 (1958).

[2] T. J. Silva, C. S. Lee, T. M. Crawford, and C. T. Rogers, J. Appl. Phys. **85**, 7849 (1999), A. B. Kos, T. J. Silva, and P. Kabos, Rev. Sci. Instrum. **73**, 3563 (2002).

[3] O. Karlquist, Trans. R. Inst. Tech. Stockholm **86**, 3 (1954).

[4] A. B. Kos, J. P. Nibarger, R. Lopusnik, T. J. Silva, and Z. Celinski, J. Appl. Phys. **93**, 7068 (2003).

[5] J. P. Nibarger, R. Lopusnik, and T. J. Silva, Appl. Phys. Lett. **82**, 2112 (2003).

[6] C. Kittel, *Introduction to Solid State Physics*, 7th ed. (Wiley, New York, 1995).

[7] L. Néel, Compt. Rend. **238**, 3051468 (1953).

[8] S. Ingvarsson, L. Ritchie, X. Y. Liu, Gang Xiao, J. C. Slonczewski, P. L. Trouilloud, and R. H. Koch, Phys. Rev. B **66**, 214416 (2002).

[9] S. Chikazumi, *Physics of Magnetism* (Krieger, Malabar, FL, 1964), p. 52.

[10] R. K. Wangsness, Phys. Rev. **91**, 1085 (1953).

[11] M. Farle, A. N. Anisimov, K. Beberschke, J. Langer, and H. Maletta, Europhys. Lett. **49**, 658 (2000).

[12] M. Kowalewski, W. H. Butler, N. Moghadam, G. M. Stocks, T. C. Schulthess, K. J. Song, J. R. Thompson, A. S. Arrott, T. Zhu, J. Drewes, R. R. Katti, M. T. McClure, and O. Escorcia, J. Appl. Phys. **87**, 5732 (2000).

[13] R. M. Bozorth, *Ferromagnetism* (IEEE, New York, 1978).

[14] C. Schober and V. N. Antonov, Phys. Status Solidi B **143**, K31 (1987).

[15] G. E. Grechnev, N. V. Savchenko, I. V. Svechkarev, M. J. G. Lee, and J. M. Perz, Phys. Rev. B **39**, 9865 (1989).

Iron and Permalloy based magnetic monolithic tunable microwave devices

Bijoy Kuanr,[a] L. Malkinski, R. E. Camley, and Z. Celinski
Department of Physics, University of Colorado at Colorado Springs, Colorado Springs, Colorado 80933-7150

P. Kabos
Radiofrequency Division, National Institute of Standards and Technology, 325 Broadway, Boulder, Colorado 80305

(Presented on 15 November 2002)

We fabricated a series of magnetic monolithic tunable microwave notch-filters and phase shifters. In contrast to previous work with molecular beam epitaxy grown metallic ferromagnets, our devices were created by magnetron sputtering. Single crystal GaAs (001) was used as a substrate. Iron and Permalloy were used as magnetic materials in a coplanar waveguide geometry. The transmission characteristics of the filters were observed to depend on substrate quality, film deposition parameters (Argon pressure, growth rate, power, etc.), and grain size. In addition we observed a substantial increase in the resonance frequency for the Fe based notch-filters. This increase in the resonance frequency is due to a growth-induced uniaxial anisotropy field of 40 kA/m in the Fe films. This is an unexpected and important result especially because the observed anisotropy is growth and not field induced. The resonance frequency shifted from 9.3 GHz at zero applied magnetic field to 15 GHz for an applied static magnetic field as low as 72 kA/m (0.9 kOe). The Fe based notch filter attenuation was greater than 35 dB/cm over the whole applied field range at the resonance condition. The phase shift of the Fe structures was up to 100°/cm at 8 GHz. The Permalloy based filters show, over the same magnetic field range, a shift in the resonance frequency from 2 to 9 GHz. The attenuation of the Permalloy filters at resonance (6 dB/cm) is substantially lower than in the Fe based filters. © 2003 American Institute of Physics. [DOI: 10.1063/1.1557856]

INTRODUCTION

The development of hybrid structures formed by thin metallic magnetic films, e.g., Fe, Permalloy, etc., on semi-insulating substrates[1-4] has received considerable attention as a technique for integrating microwave devices with semiconductor technology. This allows construction of high frequency microwave and millimeter wave monolithic integrated circuits (MMIC). In this article we concentrate on the coplanar waveguide (CPW) structure, because it is especially suitable for the magnetic-MMIC design, due to the easy implementation of additional microwave components without via holes.[3]

Recent work on magnetic-MMIC has focused on the use of metallic ferromagnetic materials because their high saturation magnetization allows for operation of the devices at higher frequencies than with conventional insulating ferrites. Most of the ferromagnetic metal-based MMIC devices fabricated up to now have used molecular beam epitaxy (MBE) growth, a process that is generally not compatible with industrial mass production techniques. In contrast, we report here on the manufacturing of magnetic MMIC devices by magnetron sputtering, a technique widely used in the industry. The magnetron sputtering has an additional advantage. While MBE grown films are generally thin, on the order of 100 nm or less, the microwave MMIC devices often require films with thicknesses that are much larger, on the order of 1

to 2 μm or so. This is because the film thickness should generally be comparable or larger than the skin depth in magnetic material. This thickness can be more easily achieved by sputtering techniques.

EXPERIMENTS

The CPW lines were fabricated by depositing thick magnetic layers of either Fe (650 nm) or Permalloy (750 nm) on top of insulating GaAs substrates to reduce the microwave loss. A thin 10 nm Ti film was used to increase adhesion. The background pressure in our deposition system was 13 μPa (1.0×10^{-7} Torr). The deposition was made using an rf/dc magnetron source at a rate of ~0.1 nm/s and with argon (Ar) pressure 0.27–0.53 Pa (2–4 mT). A thin layer of Ag was deposited on top to prevent oxidation of the magnetic film. The films were photolithographically patterned followed by ion milling in an Ar atmosphere. The CPW structure was designed for a characteristic impedance of 50 Ω. Two right-angle bends are introduced at the ends of the transmission line to allow for the commercial microprobes to make contact, and also make the component of the oscillating radiofrequency microwave field, h_{rf}, perpendicular to the applied bias static magnetic field.[5] In this geometry the energy of the electromagnetic wave propagating along the CPW structure is coupled into the magnetic films and incurs ferromagnetic resonance phenomena. The resulting resonance frequency can then be tuned by varying the external magnetic field.

We characterized the CPW transmission lines at frequencies from 0.5 to 20 GHz using an automated vector network-
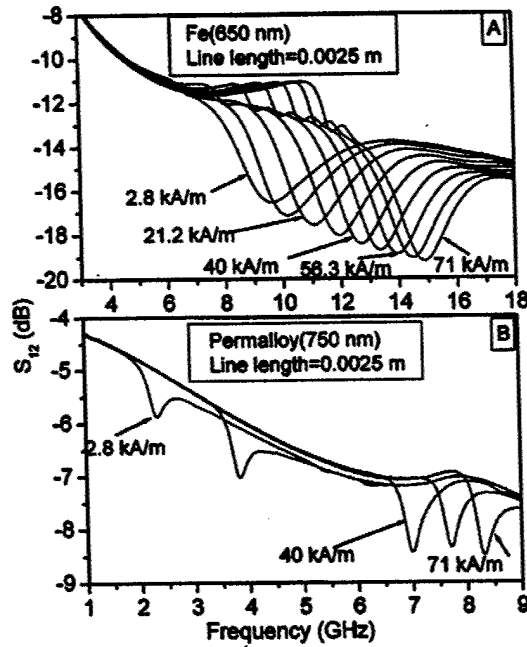

FIG. 1. Attenuation for Fe (a) and Permalloy (b) based coplanar waveguides as a function of frequency for different applied fields.

analyzer (VNA) and a microprobe station; the on wafer calibration was done using the NIST Multical® software for the through-short-line (TRL) calibration procedure.[6] The longest and the shortest lines used for calibration were 0.0071 and 0.0025 m to cover the entire frequency range of interest.

RESULTS AND DISCUSSION

Figure 1 shows the on-wafer calibrated transmission scattering matrix coefficient S_{21} as a function of frequency for Fe (a) and Permalloy (b) 0.0025 m long CPW lines. The transmitted signal shows a dip at the ferromagnetic resonance frequency due to the coupling of microwave energy to the magnetic spin system. For an isotropic material this resonance frequency (f_{res}) is given by

$$f_{res} = \left(\frac{|\gamma|}{2\pi}\right)\sqrt{H(H+M_s)},\qquad(1)$$

where H is the applied field, M_s is the saturation magnetization, and γ is the gyromagnetic ratio $|\gamma|=2.31 \times 10^8$ m/kA s. The observed resonance frequency of 9.53 GHz for the Fe CPW with saturation magnetization of $\mu_0 \times M_s = 2$ T, with $\mu_0 = 4\pi \times 10^{-7}$ H/m as the permeability of the vacuum, and a bias field of 2.4 kA/m (0.03 kOe) does not follow the prediction from Eq. (1). We determined that our deposited Fe film had a substantial uniaxial anisotropy field, H_U, along the direction of the applied static bias field. If the uniaxial anisotropy, with an easy axis oriented along the applied static bias field, is taken into account the resonance frequency is given by

$$f_{res} = \left(\frac{\gamma}{2\pi}\right)\sqrt{(H+H_U)(H+M_s+H_U)}.\qquad(2)$$

The presence of the uniaxial anisotropy is important for possible applications. If one would be able, during the process of the deposition, to align the easy axis parallel to the center-conductor of the CPW it would allow the initial resonance frequency (the frequency when $H=0$) of magnetic MMIC devices to be controlled. We will address this issue more closely later in the text. At the moment, we wish to emphasize that the experimental results for the Fe CPW devices show a significant uniaxial anisotropy even though they were made by magnetron sputtering.

We followed the resonance behavior of the magnetic-MMIC devices by measuring the calibrated two-port scattering matrix coefficients S_{ij} of the particular device while tuning the resonance frequency of the device up to 15 GHz by applying a small external magnetic field from 0 to 72 kA/m (0.9 kOe). From the measured scattering transmission matrix coefficient S_{21} we estimated that the attenuation at resonance for the Fe CPW filter was ~ 35 dB/cm in the entire applied magnetic field range. As seen in Fig. 1(a), the total loss in the measured device has an additional nonmagnetic insertion loss of 12 dB that will be addressed later in the text.

In contrast, the transmission scattering matrix coefficient S_{21} for the Permalloy-based CPW filter, shown in Fig. 1(b), exhibits resonance at a much lower frequency that the Fe-based filters for the same magnetic bias field. For example, for the bias field of 2.4 kA/m (0.03 kOe), the resonance is at 2.3 GHz in the Permalloy devices while it is 9.5 GHz for the Fe-based devices at the same applied field. This decrease in the resonance frequency is due to the smaller saturation magnetization $\mu_0 \times M_s = 1$ T along with a much smaller uniaxial anisotropy typical of Permalloy films. The resonance frequency in the Permalloy CPW was tuned up to 8.5 GHz by increasing the bias field up to 72 kA/m (0.9 kOe). The resonance attenuation obtained for this filter is ~ 10 dB/cm with an additional nonmagnetic insertion loss of ~ 7 dB.

The investigated magnetic MMIC CPW filters show some performance limitations that will have to be addressed in the future. These are mainly the nonmagnetic insertion loss as well as the background frequency dependence of the devices. The limitations are primarily due to the construction design of the CPW line; the sharp 90° turns are a source of radiation losses and substrate mode generation which contribute to the observed nonmagnetic insertion loss and the smoothness of the transmission curve. Since the skin depth becomes comparable to the conductor thickness below 20 GHz, the field penetration effects are also important in the entire frequency range studied.

Figure 2 shows the dependence of the resonance frequency on the applied bias static magnetic field. The solid line represents the theoretical calculation using Eq. (2) and the symbols show the experimental results. To fit the experimental data for the Fe CPW filter we had to use a relatively large uniaxial anisotropy of 37. 6 kA/m (0.47 kOe). As already mentioned above, this is a surprising result since one would expect isotropic behavior in sputtered devices. We attribute this to the effect of the single crystal (001) oriented GaAs substrate, which was apparently slightly miscut. The Permalloy samples that were grown on a different set of
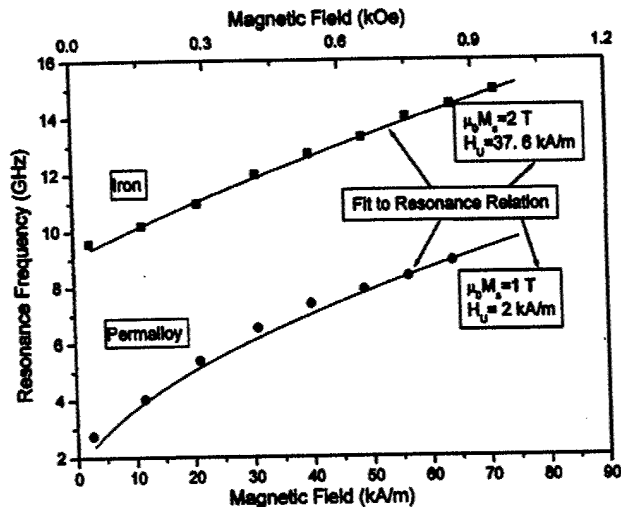
J. Appl. Phys., Vol. 93, No. 10, Parts 2 & 3, 15 May 2003

Kuanr *et al.*   8593

FIG. 2. Resonance frequency as a function of applied field for Fe and Permalloy.

FIG. 3. Transmitted phase (a) as a function of frequency for Fe based devices, and phase shift (b) as a function of applied magnetic field.

GaAs substrates showed only a very small growth-induced magnetic anisotropy.

The misorientation of the GaAs substrate introduced a growth-induced anisotropy in the Fe films during the deposition. Earlier experiments[4] with MBE grown ultrathin Fe films (3 nm and below) on the same single crystal GaAs substrates also showed very large anisotropies, up to 160 kA/m (2 kOe). Angular FMR measurements proved that the observed anisotropies in the MBE grown films were uniaxial in nature. The fact that our sputtered films were much thicker that the MBE grown films, and still showed significant anisotropy, indicates that the single crystal GaAs substrate induces stresses throughout the Fe film, resulting in a large uniaxial anisotropy field H_U.

The large uniaxial anisotropy in the Fe structures could be very important for device development since it boosts the operational frequency substantially. It is interesting to speculate whether a deliberately miscut substrate could be utilized in the future design of sputtered thin film magnetic-MMIC devices. Additional research should be done to explore the possibility of obtaining even larger uniaxial anisotropies in sputtered Fe films by proper orientation of single crystal GaAs substrates, possibly in combination with deposition in a magnetic field.

The CPW notch filters can also be used, in principle, as phase shifters. The results for phase shifter operation are presented in Fig. 3 for the Fe-based CPW structures. The top panel shows the phase angle of the transmitted signal as a function of the frequency for different values of the applied field. Although substantial changes are seen near resonance, the attenuation of the device at these frequencies is high (the device performs as a notch filter close to resonance) which makes operating the device as a phase shifter unsuitable at these frequencies. By close inspection of the measured data, we observed that away from the resonance there is still a shift of the phase angle with the applied field. This change in phase angle away from resonance, as a function of the ap-
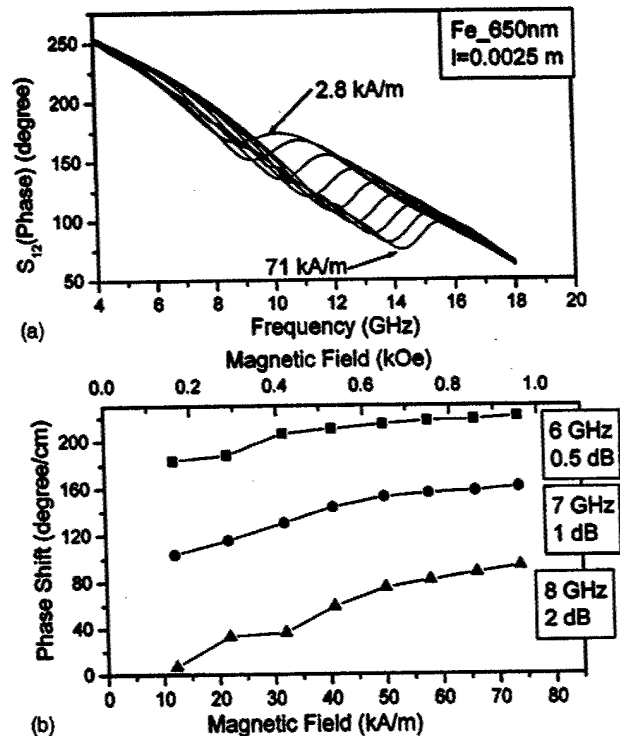
plied field, is plotted in Fig. 3(b). Note that at 8 GHz, a phase shift of 100 deg/cm was measured with only a 2 dB change of insertion loss. At lower frequencies the observed attenuation as well as the phase change are both smaller.

In conclusion, we constructed a set of microwave devices using Fe and Permalloy grown by magnetron sputtering. From the observed data we can conclude that devices grown by magnetron sputtering have performance characteristics that are similar to the characteristics of devices grown by MBE. An intriguing development is the observed large uniaxial anisotropy in sputtered materials. This growth-induced anisotropy is important from the device design standpoint because it can significantly increase the operational frequency of microwave ferromagnetic metal devices.

[1] E. Schloemann, R. Tuistison, J. Weissman, H. J. Van Hook, and T. Varitimos, J. Appl. Phys. **63**, 3140 (1988).

[2] V. S. Liau, T. Wong, W. Stacy, S. Ali, and E. Schloemann, Proc. IEEE MTT-S IMS, 957 (1991).

[3] J. Su, C. S. Tsai, and C. C. Lee, J. Appl. Phys. **87**, 5968 (2000).

[4] N. Cramer, D. Lucic, R. E. Camley, and Z. Celinski, J. Appl. Phys. **87**, 6911 (2000).

[5] N. Cramer, D. Lucic, D. K. Walker, R. E. Camley, and Z. Celinski, IEEE Trans. Magn. MAG-37, 2392 (2001).

[6] Roger B. Marks, IEEE Trans. Microwave Theory Tech. **39**, 1205 (1991).

Exchange bias in the Fe/KCoF$_3$ system: A comprehensive magnetometry study[a]

L. Malkinski[b]
Department of Physics, University of Colorado at Colorado Springs, 1420 Austin Bluffs Parkway, Colorado Springs, Colorado 80918 and University of New Orleans, AMRI, New Orleans, Louisiana 70148

T. O'Keevan, R. E. Camley, and Z. Celinski
Department of Physics, University of Colorado at Colorado Springs, 1420 Austin Bluffs Parkway, Colorado Springs, Colorado 80918

L. Wee and R. L. Stamps
Department of Physics, University of Western Australia, 35 Stirling Highway, Crawley, WA 6007, Australia

D. Skrzypek
University of Silesia, Institute of Physics, Uniwersytecka 4, Katowice 40-007, Poland

(Presented on 12 November 2002)

Exchange bias was studied in the Fe/KCoF$_3$ ferromagnet/antiferromagnet system. KCoF$_3$ can be deposited onto single crystal of Fe, either in the polycrystalline or single crystal form, depending on growth conditions. The samples were grown by molecular beam epitaxy on Ga-terminated GaAs (100) wafers. We study effects of the crystal state of the fluoride, thickness of the Fe film, crystallographic orientation of the Fe, and temperature on exchange bias. The structures with single crystal KCoF$_3$ show that the exchange bias is well correlated with the coercivity at low temperatures and vanishes at a temperature close to the Néel temperature. Both the magnitude of the exchange bias and the blocking temperature of the samples with the polycrystalline fluoride were significantly reduced compared to the single crystal structures. As the Fe film thickness was increased, the exchange bias decreased for all samples. In contrast, the blocking temperature remained unchanged for the samples with the single-crystal fluoride. The exchange bias measured along the easy anisotropy axis of the Fe was slightly larger than that measured along the hard axis. In addition, all samples exhibited a weak training effect. © *2003 American Institute of Physics.*
[DOI: 10.1063/1.1558653]

The exchange bias originates from exchange interactions among magnetic atoms at the ferromagnet/antiferromagnet interface and it manifests itself as a shift of magnetization hysteresis loops. It also contributes to magnetic anisotropy as a unidirectional anisotropy component and can be measured using torque magnetometry or ferromagnetic resonance techniques. In spite of numerous works on exchange bias systems during the past decade the mechanism of exchange bias is still not fully understood.[1–4]

Exchange bias exists in a variety of nanostructured systems including granular and layered structures. The system we studied consists of a single crystal (100) Fe film and a KCoF$_3$ film, which is a model Heisenberg antiferromagnet. The key feature of this system is that the antiferromagnet can be grown on the Fe film in either single crystal or polycrystalline forms. It has been recently found that the crystalline form of the fluoride significantly modifies magnetocrystalline anisotropy of the adhering Fe film.[5,6] This article is devoted to a comprehensive study of exchange bias in this interesting system.

A molecular beam epitaxy system was used to deposit the exchange bias system. A few monolayers of Fe were deposited on a Ga terminated (100) GaAs substrate as a seed

layer. Then, single crystal (100) Fe films with thicknesses from 1 to 3 nm were deposited on 80 nm Ag templates. Films of KCoF$_3$ with a thickness of 30 nm were deposited onto the Fe layer using an electron-gun evaporator. Single crystals of KCoF$_3$ grow at low deposition rates (below 0.1 nm/s) and at elevated temperatures (~180 °C). Room temperature deposition with the rates above 0.2 nm/s resulted in a columnar growth of polycrystalline film, with a typical diameter near 5 nm. Moreover the direction of growth for these columns varies from grain to grain. For the single crystal KCoF$_3$ a typical lateral grain size is significantly larger (above 50 nm) but dislocation defects at the Fe/fluoride interface are visible, separated by distances of 20–50 nm. The exchange bias was measured for 5 K $\leq T \leq$ 300 K, using a SQUID magnetometer. In addition some results were verified by ferromagnetic resonance measurements at 24 K.

Typical magnetic hysteresis curves measured along the easy and hard axis are presented in Fig. 1 for the sample with 1.3 nm thick Fe (001) and a single crystal KCoF$_3$. They are superpositions of hysteresis loops representing the two Fe layers. The central part of the loop refers to the exchange-biased Fe layer and it consists of two magnetization jumps, which are asymmetric with respect to the zero field. The approach to magnetic saturation at higher fields reflects magnetization behavior of the thinner seed layer, which is separated by a thick Ag buffer layer from the exchange biased
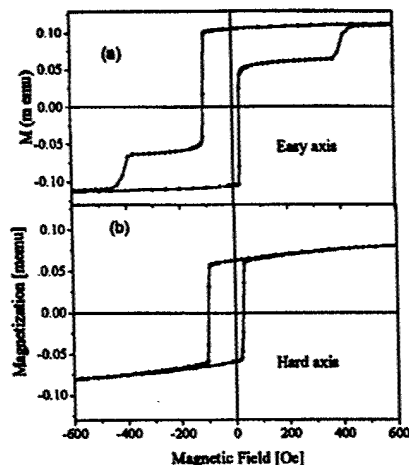

FIG. 1. Hysteresis loops for the single crystal Fe/KCoF$_3$ bilayer deposited on Ag template with 5 monolayers thick Fe seed layer. Magnetic field during cooling and measurement was applied along: (a) easy magnetization axis [001] and (b) hard magnetization direction [011] for Fe (001).

layer. Note that the high field jumps are symmetric about zero and not biased.

It is worth noting that the Fe seed layer shows abrupt magnetization reversal when magnetized along the easy magnetization direction and there is a gradual change and a substantially smaller hysteresis in the case of the magnetic field applied along the hard axis. This behavior of the seed layer is characteristic of single domain magnetization. In contrast the thicker exchange-biased layer does not exhibit such distinct differences for different crystallographic orientations with respect to applied field, which seems to indicate its multidomain structure. Our studies are focused on the layer showing exchange bias effects, therefore the magnetic behavior of the seed layer will be skipped in the further discussion.

We measured the temperature dependence of the exchange bias for several samples with Fe thicknesses varying from 1.05 to 2 nm. Typical results for the samples with single crystal and polycrystalline fluoride are presented in Fig. 2. In
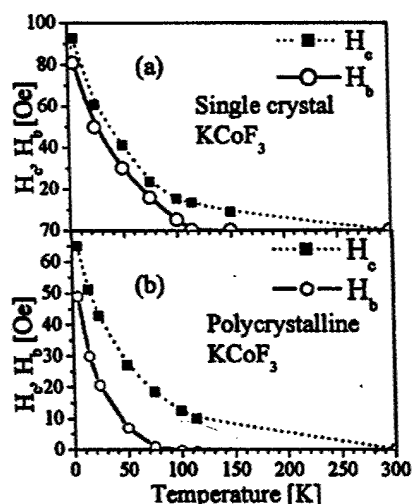

FIG. 2. Temperature dependences of coercive force (H_c) and exchange bias (H_b) for Fe/KCoF$_3$ structures with single crystal Fe and (a) single crystal fluoride and (b) polycrystalline fluoride.
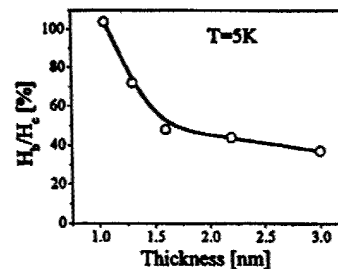

FIG. 3. The dependence of exchange bias to coercivity (H_b/H_c) ratio on the Fe film thickness in samples with single crystal fluoride. SQUID measurements were done at 5 K.

both cases the thickness of the Fe (001) film is 1.05 nm. These SQUID measurements were additionally verified by ferromagnetic resonance measurements for selected samples at 24 K. We found reasonably good agreement between the shift of the hysteresis loop and unidirectional anisotropy evaluated from the anisotropy curves measured by ferromagnetic resistance.

We found that for the samples with single crystal fluoride, there is a good correlation between temperature dependences of the coercivity and the exchange bias with a similar decrease with temperature as demonstrated in Fig. 2(a). Actually such correlation is expected for exchange bias systems in single domain models[7] because both quantities are functions of the magnetization, anisotropy, and thickness of the constituent magnetic layers. The exchange bias to coercivity ratio for the thinnest samples was in the range from 90% to 104% at 5 K and it decreased to zero at the temperature close to the Néel temperature (114 K). In contrast, samples with polycrystalline fluoride had a smaller initial exchange bias compared to the coercive field (65%–90%) and it decreased much faster with the increasing temperature as seen in Fig. 2(b). As a result the blocking temperature was substantially lower (from 50 to 75 K).

Samples deposited on GaAs wafers with different roughness had significantly different coercivities measured at 5 K—H_c varied from 65 Oe for epitaxy-ready GaAs substrates to over 300 Oe for the roughest substrate surfaces. The enhancement of the coercivity for rougher substrates can be explained by perturbed growth of the film on such surfaces and consequently increased number of defects, which obstruct domain wall movements. Because of the scatter in coercivity values on one hand and correlation between exchange bias and coercivity on the on the other, we indicated in our initial articles[5,6] that selected samples with polycrystalline fluoride (with high H_c) had larger exchange bias than those with single crystalline KCoF$_3$, however the ratio H_b/H_c for the large group of samples measured is larger for the single crystalline fluoride. This fact is demonstrated in Fig. 3, which shows the H_b/H_c ratio dependence on the thickness of the Fe film for the single crystal fluoride samples. Since we made a few samples with each thickness the points in the graph represent averaged results for samples with the same thickness. The ratio of exchange bias to coercivity decreases quickly from 104% to about half of this value as the Fe layer thickness is increased by only 4 atomic layers. Surprisingly, decay of exchange bias is much slower for larger thicknesses of Fe and it is still above 35% for
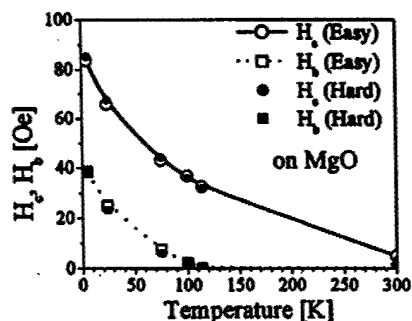
FIG. 4. The temperature dependence of coercivity and exchange bias for single crystal Fe/KCoF$_3$ bilayer deposited on MgO substrate.
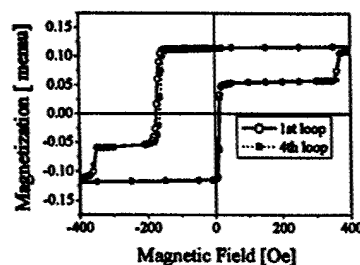

FIG. 5. Training effect in the exchange biased structure. Dashed line and filled squares represents the fourth cycle of the hysteresis loop. The sample with 1.05 nm of Fe and 30 nm single crystal fluoride was deposited on epitaxy-ready GaAs.

samples as thick as 3 nm. This suggests that the dependences of the coercivity and exchange bias on thickness (d) does not both follow the $1/d$ law[7] as for the majority of exchange bias systems.[7,8] Our data indicate that the exchange bias follows the $1/d$ dependence reasonably well while the coercivity does not. One possibility to explain this is that the exchange bias is an interface phenomenon while the coercivity of the Fe film depends on both interface and bulk effects. This idea is supported by the fact that there is no dramatic change in the coercivity around the Néel temperature.

The samples with the polycrystalline fluoride showed similar decay of the H_b/H_c ratio with the Fe thickness for the thinnest Fe films, however their results were reduced compared to those for the samples with the single crystal KCoF$_3$. One possibility to explain this is that above 1.5 nm the interface topography between the Fe and the fluoride remains the same while below this thickness the interface roughness could change with Fe thickness. The exchange bias depends on the direction of the applied field with respect to the crystallographic axes. Both the coercive field and exchange bias were about 10% smaller when measured along a hard anisotropy axis (110) than those measured along an easy magnetization direction (100).

To understand the role of the substrate, we deposited a Fe/KCoF$_3$ structure with 10 monolayers of Fe and 30 nm of single crystal fluoride on an MgO substrate with a similar Fe seed layer and Ag template. In Fig. 4 we again plot the behavior of the bias and coercive fields as a function of the temperature. In this case the exchange bias curve was again parallel to the coercivity curve and it again approached zero close to 114 K, but the decay of the coercivity had a slightly different character than that for the films deposited on GaAs. For the sample on the MgO substrate, the coercivity and exchange bias do not depend on the crystallographic direction. Coercivity at the Néel temperature decreased to only about half of its low temperature value and it was distinctly larger at room temperature than that for the samples deposited on GaAs. This suggests that magnetoelastic effects may be responsible for the observed differences in the temperature dependence of coercivity and exchange bias for samples deposited on different substrates. This interpretation involves different mismatches between the substrate and template structures and different thermal expansion coefficients for GaAs and MgO substrates. Magnetoelastic effects may be quite an important factor for understanding this behavior because of the giant magnetostriction of KCoF$_3$.[8,9]

It is also important to mention that samples with the polycrystalline or the single crystal antiferromagnet followed the theoretical prediction of a model for the temperature dependence of exchange bias only if unstable grains play a substantial role.[10] However, in this case one expects the blocking temperature to be substantially below the Néel temperature, which is not observed for the single crystal sample. We note that the temperature dependence of the exchange bias is a very rich and complex phenomenon and can depend significantly on the grains and magnetic properties of the ferromagnet and antiferromagnet.[11] After a few hysteresis loops one of the hysteresis branches was shifted toward lower fields by a few Oersteds. The positive branch of the hysteresis loop remained unchanged as illustrated in Fig. 5. In the case of FMR measurements, a few rotations of the bias field were enough to significantly reduce the unidirectional anisotropy. This reduction in exchange bias was from 5% to 7%. This behavior is consistent with our interpretation[12] based on Kouvel's model.[13] As expected, there is no training effect for the seed layer—magnetization reversal at higher fields is unaffected by the number of cycles. Both poly- and single-crystal fluoride samples exhibited a similar training effect. This is curious in that one normally associates training with a distribution of pinning sites and local anisotropies. One might expect that the distribution should narrow for the single crystal film and widen for the polycrystalline film. One possibility is that the training may be most strongly affected by defects at the interface region, which exist in both the poly- and single-crystal fluoride structures.

[1] J. Nogués and I. K. Schuller, J. Magn. Magn. Mater. **92**, 203 (1999).
[2] A. E. Berkowitz and K. Takano, J. Magn. Magn. Mater. **200**, 552 (1999).
[3] M. Kiwi, J. Magn. Magn. Mater. **234**, 584 (2001).
[4] R. Stamps, J. Phys. D **33**, R247 (2000).
[5] L. Malkinski et al., J. Magn. Magn. Mater. **240**, 261 (2002).
[6] L. Malkinski et al., J. Appl. Phys. **91**, 7242 (2002).
[7] C. Mauri et al., J. Appl. Phys. **62**, 3047 (1987).
[8] R. C. O'Handley, in *Modern Magnetic Materials*, (Wiley, Canada, 2000), Chap. 12.
[9] J. Julliard and J. Nouet, Rev. Phys. Appl. **10**, 357 (1975).
[10] M. D. Stiles and R. D. Mc Michael, Phys. Rev. B **60**, 12950 (1999).
[11] C. Hou et al., Phys. Rev. B **63**, 024411 (2001).
[12] L. Wee, thesis, University of Western Australia, 2002.
[13] J. S. Kouvel, J. Phys. Chem. Solids **24**, 795 (1963).

Hexagonal lattice of 10-nm magnetic dots

L. Malkinski[a]
University of New Orleans, AMRI, New Orleans, Louisiana 70148

R. E. Camley and Z. Celinski
Department of Physics, University of Colorado at Colorado Springs, Colorado 80919

T. A. Winningham
Department of Physics, University of Central Florida, Orlando, Florida 32816

S. G. Whipple and K. Douglas
Department of Physics, University of Colorado, Boulder, Colorado 80309

(Presented on 13 November 2002)

We have grown precisely ordered and precisely located arrays of ultra-small magnetic dots. The nanofabrication process is based on the use of a protein crystal etch mask which is used to create a hexagonal lattice of holes in Si substrates. An assembly of $(Fe/Pd)_4$ dots with the average dot size of 10 nm in diameter, 6.5 nm height, and an average separation between dot centers of 22 nm was grown using molecular-beam epitaxy. The dot locations are determined by the biological mask that is used to create ordered arrays of ~4 nm deep holes in Si. Fe/Pd multilayers (1 nm thick Fe and 0.4 nm thick Pd layers) were deposited to create dots within these holes. The dots extend ~2.5 nm above the surface, with a thicker (1.5 nm) final layer of Pd for protection of these structures during measurements. Magneto-optical Kerr effect and magnetometry data showed that these objects are magnetic even at room temperature and are fairly soft with a coercive field of ~40 Oe. Measurements of the hysteresis loop revealed that magnetization is in plane and that $4\pi M_{eff}$ is on the order of 15 kG. © 2003 American Institute of Physics. [DOI: 10.1063/1.1543861]

INTRODUCTION

During the last two decades, the use of ultrahigh vacuum technology has made possible the creation of ultrathin magnetic structures with interfaces that are sharp on the atomic scale. This development has brought not only other ways of engineering artificial magnetic materials but also exciting discoveries such as exchange coupling, giant magnetoresistance, and magnetic tunneling.[1] As a result, the significant interest by industry in different magnetic materials and devices has rejuvenated activities in the field of ultrathin magnetic structures.

One issue of paramount importance is the patterning of ultrathin magnetic structures into objects of nanometer scale[2] and the study of their static and dynamic properties. There are techniques, such as electron-beam or x-ray lithography, which make such patterning possible, although there are significant restrictions. For example, electron-beam lithography can make objects on a scale of 10 nm, but its time-intensive serial nature makes large-area patterning with this technique unfeasible. X-ray photolithography requires use of synchrotron radiation, which is not commonly accessible. The aim of our work was to grow patterned magnetic structures using a biologically derived parallel fabrication technique and to study the magnetic properties of the structures. This approach allowed us to create large areas of patterned magnetic structures (~cm²). In this article, we describe in detail the preparation of Si wafers, the growth process, and the results

of superconducting quantum interference device magnetometer (SQUID) and magneto-optical Kerr effect (MOKE) measurements on a regular hexagonal array of 10 nm in diameter $(Fe/Pd)_4$ magnetic dots.

SAMPLE PREPARATION

The growth process is based on the use of two-dimensional protein crystals as an etch mask. The preparation of the protein crystals and their use as masks have been described in previous publications.[3–6] They are native two-dimensional crystals that form the surface layer (S layer) of the archaebacteria sulfolobus acidocaldarius. They possess a hexagonal array of pores with a 22 nm lattice constant and pore diameters of 10 nm. The size of the native protein crystal fragments is on the order of 1 to 2 μm in diameter.

The protein crystals were applied to the Si wafer in an aqueous suspension. The density of the surface coverage is controlled by regulating the protein concentration in the aqueous suspension. The Si substrates used in our studies were approximately 50% covered with S layers, which insured that we avoided overlapping protein crystal fragments. After a short drying process, the Si wafers were placed in an electron-beam deposition system where a layer of Cr was deposited under an angle of approximately 60°. The periodic topography of the protein crystals produced a shadow at each pore site, effectively creating an ordered array of holes in the deposited Cr film. Inductively coupled plasma was used to transfer the pattern of the protein crystals into the Si substrate in the form of an ordered array of holes, verified by atomic force microscopy (AFM). Areas not covered by Cr
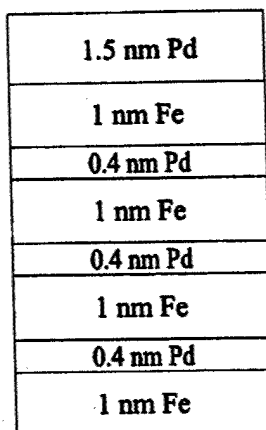
[a]Electronic mail: lmalkins@brain.uccs.edu

| 1.5 nm Pd |
| 1 nm Fe |
| 0.4 nm Pd |
| 1 nm Fe |
| 0.4 nm Pd |
| 1 nm Fe |
| 0.4 nm Pd |
| 1 nm Fe |

FIG. 1. A schematic diagram of the individual magnetic dot.

FIG. 2. Atomic force microscopy image of $(Fe/Pd)_4$ magnetic dots grown on a Si substrate. The thickness of an individual Fe layer within a dot was 1 nm, the thickness of Pd between Fe layers was 0.4 nm, and the dots were capped with a 1.5 nm thick Pd layer.

are etched while those with Cr are protected. The size of the holes was adjusted by varying the etch parameters and time. These Si substrates, with the Cr/protein crystal mask still in place, were introduced into the ultrahigh vacuum deposition system.

We grew the arrays of magnetic dots at room temperature in a molecular-beam epitaxy system.[7] Using Knudsen cells, we deposited four 1 nm thick Fe layers separated by 0.4 nm thick Pd layers. The final Pd layer was 1.5 nm thick to prevent oxidization during measurements in ambient condition. Figure 1 shows a schematic diagram of our individual magnetic dot. The thicknesses of the individual layers and the rate of growth (~ 0.1 nm/min) were monitored by a thickness monitor. In addition to the patterned Si substrate, we deposited a control sample directly on bare unpatterned Si. Despite the fact that the Si substrates were introduced to the molecular-beam epitaxy system with the protein mask on them, we did not observe an increase of the base pressure, indicating that outgassing was minimal. After deposition, we removed the protein mask leaving arrays of $(Fe/Pd)_4$ dots on the Si substrates.

AFM measurements were made in air using a Digital Instruments Nanoscope III operating in tapping mode (Fig. 2). Dot diameters were on the order of 10 nm. Because we have not yet optimized our mask removal technique, defects and missing dots can be found in the array, most likely created during the removal or liftoff process. Magnetic force microscopy measurements were attempted, but preliminary efforts have been unsuccessful. We have had difficulty getting the resolution below 30 nm, and thus have not been able to image individual dots with magnetic contrast.

MAGNETIC MEASUREMENTS

Before presenting the magnetic results we would like to comment on the question of superparamagnetic behavior in these structures. The prepared magnetic dots are very small (10 nm in diameter and 6.5 nm in height). Pure iron objects with such small dimensions are superparamagnetic above approximately 50 K since thermal fluctuations are much larger than the anisotropy energy. To increase the blocking temperature one needs to introduce an additional anisotropy to
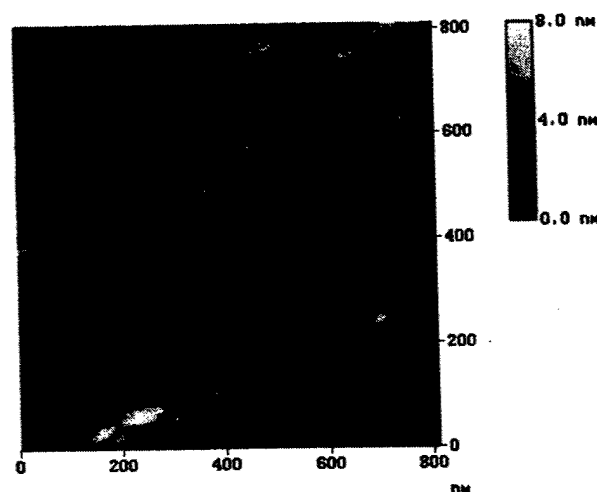
the structures. By layering the Fe with Pd, nine Pd/Fe interfaces were created which significantly increased the effective anisotropy.[8] Furthermore, the 0.4 nm thick Pd interlayer between the Fe layers produces a strong ferromagnetic coupling between the Fe films, and each dot thus responds as a single magnetic unit.[9]

We conducted a series of magnetic measurements using a MOKE system and a SQUID magnetometer. Both techniques revealed that the system is ferromagnetic even at room temperature because a coercive field was observed. The shape of the hysteresis loops was very different for the patterned samples than that observed for samples with a continuous film (see Fig. 3). For the continuous film structures we observed a square hysteresis loop with a coercive field of 10 Oe; the patterned structures exhibited S-shape hysteresis loops with larger coercive fields (on the order of 35 Oe).
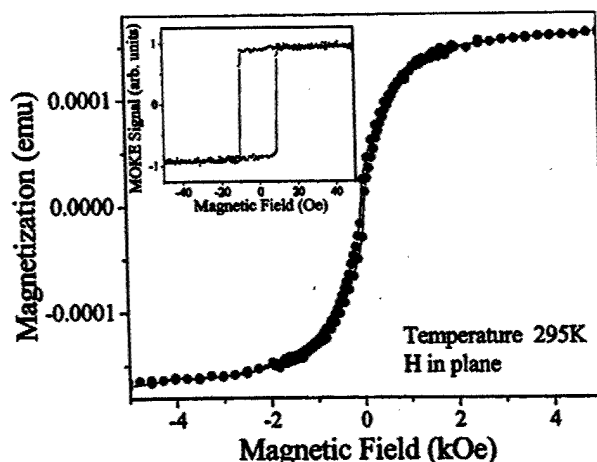

FIG. 3. Hysteresis loop for the magnetic dot array measured at 295 K with the magnetic field applied in the plane of the structure. Inset shows data for identical continuous film structure. Note the squareness of the hysteresis loop for the continuous film structure.
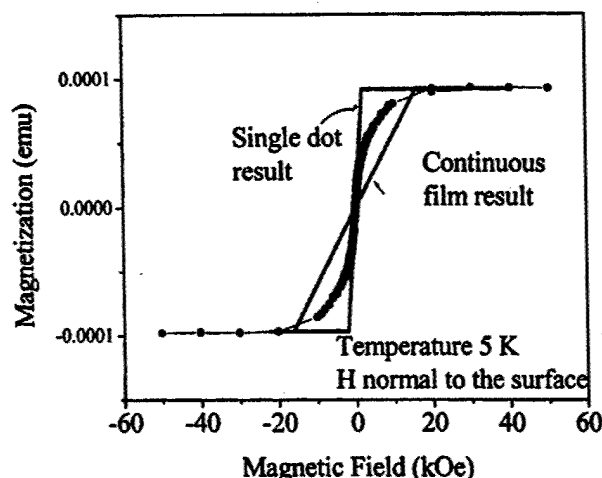
FIG. 4. Hysteresis loop measured at 5 K with the magnetic field applied normal to the sample plane. The solid lines represent theoretical calculations of the magnetization vs field for the continuous film structure and for an array of independent dots with the appropriate demagnetizing factors.
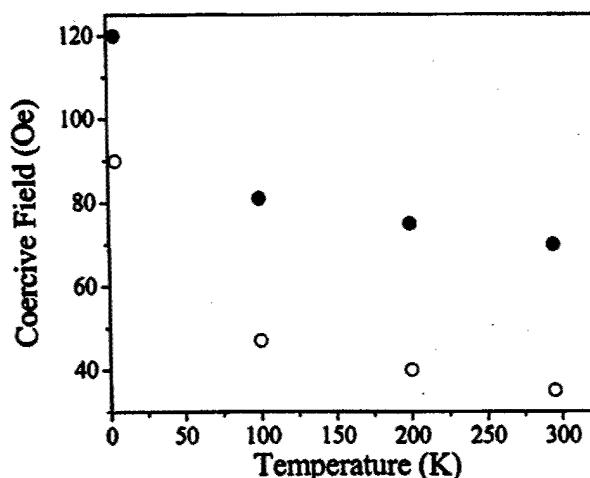

FIG. 5. The coercive field as a function of the temperature measured with the magnetic field applied in plane (open symbols) and normal (solid symbols) to the structure.

Moreover, the patterned structure requires a field of 4 kOe to reach saturation. The saturation field decreases with decreasing temperature to 3 kOe at 5 K. The coercivity increased with decreasing temperature, reaching a value of 90 Oe at 5 K. Since the samples do not exhibit translational invariance over the range larger than 2 μm, the measured response is an average for all dots in different patterned regions.

The out-of-plane measurements showed that it was necessary to apply a magnetic field larger than 15 kOe in order to saturate the sample (see Fig. 4). This indicates that the magnetization is in the plane of the sample. Moreover, the shape the hysteresis loop in this configuration is very different than that found in continuous films and also different for that expected for an array of independent dots. In Fig. 4 the solid lines represent theoretical calculations of the magnetization versus field for the continuous film structure and for an array of independent dots with demagnetizing factors $N_x = N_y = 0.24$ and $N_z = 0.52$ (where z is the axis of the cylinder).[10] The calculation for $M(H)$ for the independent dot is based on a minimization of the magnetostatic energy and Zeeman energy and assuming that the interior fields can be appropriately approximated by the demagnetizing factors. The fact that the measurements lie in between these two limits suggests that there is substantial interaction between the dots.

Figure 5 presents data on the temperature dependence of the coercivity for applied field both perpendicular and in plane. The coercivity decreases slowly as temperature increases for both configurations. This suggests that the superparamagnetic limit is well above room temperature. It is interesting to note that the coercivity is larger for the out-of-plane geometry.

In conclusion, we have grown series of ultra small $(Fe/Pd)_4$ dot arrays. The magnetic properties of the dot arrays are very different from those of the equivalent continuous films. The coercive field for the dot array is increased by a factor of three and the saturation field is increased by a factor of over 100. The out-of-plane results showed that the behavior of our system lies between that of a continuous film and an array of independent dots, indicating that the interaction between these dots is important. The presence of coercivity and the shape of the hysteresis loops indicate that these dots are magnetic even at room temperature.

[1] B. Heinrich and J. F. Cochran, Adv. Phys. **42**, 523 (1993).
[2] See, for example, J. I. Martin, J. Nogués, Kai Liu, J. L. Vicent, and Ivan K. Schuller, J. Magn. Magn. Mater., **256**, 449 (2003) and the references therein.
[3] K. Douglas, N. Clark, and K. Rothschild, Appl. Phys. Lett. **48**, 676 (1986).
[4] K. Douglas, G. Devaud, and N. Clark, Science **257**, 642 (1992).
[5] T. A. Winningham, H. P. Gillis, D. A. Choutov, K. P. Martin, J. T. Moore, and K. Douglas, Surf. Sci. **406**, 221 (1998).
[6] T. A. Winningham, S. G. Whipple, and K. Douglas, J. Vac. Sci. Technol. B **19**(5), 1796 (2001).
[7] Z. Celinski, J. Vac. Sci. Technol. A **19**, 383 (2001).
[8] B. Heinrich, Z. Celinski, J. F. Cochran, A. S. Arrott, and K. Myrtle, J. Appl. Phys. **70**, 5769 (1991).
[9] Z. Celinski and B. Heinrich, J. Magn. Magn. Mater. **99**, L25 (1991).
[10] Du Xing Chen, James A. Brug, and Ronald B. Goldfarb, IEEE Trans. Magn. **27**, 3601 (1991).

Tunable High Frequency Band Stop Magnetic Filters

Bijoy Kuanr, Z. Celinski, and R. E. Camley

Center for Magnetism and Magnetic Nanostructures

Department of Physics
University of Colorado at Colorado Springs

Colorado Springs, CO 80933-7150

ABSTRACT

We present results on Fe and Permalloy based microstrip microwave band stop filters. These structures, prepared on GaAs substrates, are compatible in size and growth process with on-chip high frequency electronics. We observed power attenuation of 100 dB/cm for Permalloy and 180 dB/cm for Fe. The insertion loss is low – 2-3 dB for Permalloy and 3-5 dB for the Fe based structures. Our geometry includes a significant boost to the zero-field operational frequency due to the shape anisotropy of the magnetic element in the microstrip. Using the shape anisotropy we create a Fe-based filter that operates at 11 GHz with zero applied field.

The frequency range of 10-100 GHz is particularly interesting for communications, military and security applications. For example, there are obvious needs to see through fog, clouds, and smoke, but this can not be done in visible light or infrared radiation. These obstacles are transparent, however, for electromagnetic waves at particular frequencies in the GHz range. Thus signal processing in this range is of significant importance.

There are a few devices that operate at high frequencies; however they are large and bulky. Recently we have witnessed incredible progress in high frequency semiconductor electronics and a movement towards the synthesis of different electronic components into integrated circuits. Here we describe new, on-wafer, magnetic devices which are small and could be integrated with high frequency electronics. Reduction of device dimensions in these monolithic microwave integrated circuits is important from the cost and reliability point of view.

The operational frequency, f, can be obtained from the ferromagnetic resonance condition and is set by material properties, such as saturation magnetization, M_s, anisotropy fields, H_a, the gyromagnetic ratio, γ, and the magnitude of an applied field, H. If the applied field is along the easy axis, the frequency is given by

$$f = \gamma\sqrt{(H + H_a)(H + H_a + 4\pi M_S)} \qquad (1)$$

and therefore the resonance frequency can be varied with an external magnetic field.

Most current devices are based on a low magnetization ferrimagnetic insulator (YIG). Our work, in contrast, uses a novel approach where high magnetization, metallic ferromagnets are the active element in these filters. This high magnetization allows the

2

high frequency operation. The table below shows theoretical results for operational frequencies for different materials.

Material	$4\pi M_s$ (kG)	Frequency (GHz) at 1 kG Applied Field
YIG	1.75	4.8
Permalloy	10.0	9.7
Fe	21.5	17.2

With YIG an applied field of over 11 kG is necessary to reach frequencies of about 35 GHz. Such large fields are incompatible with devices of a limited size since substantial electromagnets are required. Clearly the use of metallic ferromagnets would significantly increase the operational frequency.

While Fe has a much higher resonance frequency for the same applied field, its conductivity can lead to high loss at microwave frequencies. However, structures utilizing thin Fe films minimize conduction loss while still producing high attenuation at the band-stop frequency.[1-2] Early attempts at producing Fe-film-based structures have succeeded in making filters with high band-stop frequencies and low broadband loss.[1-3] However, the maximum attenuation only reached about 4–5 dB/cm. Currently, a number of different approaches have been investigated using ferromagnetic metals.[4-9]

Our theoretical calculations[10-12] indicated that attenuation in the notch filters was inversely proportional to the thickness of the waveguide. Essentially as one reduces the thickness of the dielectric a larger fraction of the electromagnetic energy density is contained in the ferromagnetic metal. At resonance this energy is easily dissipated and one obtains a larger attenuation. Based on this work, we have recently constructed microstrip

band-stop filters using a different geometry and growth method, resulting in much higher attenuation.[4-6] Most of the previous devices have been fabricated using Molecular Beam Epitaxy (MBE). In contrast, we have constructed magnetic devices grown by magnetron sputtering, a technique commonly used in industry. The sputtering technique has a second advantage. MBE grown films are generally thin, less than 100 nm, but the microwave devices require thicker films, 1-2 microns, to be on the order of the skin depth in the magnetic material. The sputtering technique is quite capable of producing these thicker films.

Here we report results on microstrip devices which exhibit strong attenuation (up to 180 dB/cm in power measurements) and low insertion loss (2-3 dB). This is accomplished by creating devices with good impedance matching which is achieved by making the microstrip line much narrower. Because the microstrip line includes the ferromagnetic material there is a second major effect, a boosting of the operational frequency due to the created shape anisotropy in the magnetic material.

In Fig. 1 we show a cross section of our device. Using sputtering we deposit the following sequence of materials on GaAs substrates. We begin by growing the bottom electrode - a 2 nm seed layer of Fe, a 2 micron thick Ag layer, a Ti layer for adhesion. The rest of the structure is grown through a shadow mask, starting with a 4 micron thick SiO_2 film , a thin Ti film for adhesion, Fe or Permalloy film (0.3 to 0.5 microns thick) followed by a thick Ag film (1.5 microns thick) . The device is patterned by photolithography and dry etched.

We determine the performance of our devices using a vector network analyzer. We characterized the microstrip transmission lines at frequencies from 1 to 40 GHz using an

automated vector network-analyzer. To remove the influence of cables, probes, etc. an on wafer calibration was done using the NIST Multical® software for the through-short-line (TRL) calibration procedure[13].

Before we present our results we estimate the effect of the shape anisotropy on the operational frequency. The magnetic material in our structure is in the form of a long ribbon with the following dimensions – length = 3 mm, width = 18 μm, thickness = 0.35 μm. This leads to the following dynamic demagnetizing factors, $N_x = 0.966$, $N_y = 0.034$, and $N_z = 0$. The formula for the resonance condition is now given by

$$f = \gamma \sqrt{\left(H + H_a + (N_y - N_z)4\pi M_s\right)\left(H + H_a + (N_x - N_z)4\pi M_s\right)} \qquad (2)$$

If we calculate the frequency at zero applied field, we find that without the shape anisotropy the frequency is zero (if $H_a = 0$) and with the shape anisotropy the frequency is about 11 GHz for the Fe structure and about 5 GHz for Permalloy. This is a substantial boost in operational frequency.

In Figure 2 we plot transmission as a function of frequency for the Py based microstrips. We first note that the zero-field frequency is slightly above 4 GHz, in reasonable agreement with the estimate above based on shape anisotropy. The insertion loss over most of the region is on the order of 2-3 dB while the power attenuation is close to values of 100 dB/cm. The width of the attenuation dip (measured at 3 dB above the minimum, i.e. half maximum) becomes distinctly narrower at higher frequencies (0.4 GHz for the dip at 20 GHz compared to a width of 0.82 GHz at 4.3 GHz). This narrowing of the width of the attenuation peak is consistent with our theoretical results as seen in the inset.

In Figure 3 we show the results for an Fe based microstrip. The zero-field frequency of about 11 GHz is in excellent agreement with the calculation based on shape

anisotropy. For the Fe-based structure the insertion loss is somewhat larger, between 3-5 dB. The power attenuation is dramatically larger, 180 dB/cm at 30 GHz. Again we seen a narrowing of the width of the attenuation dip – it is 3 GHz at 11 GHz and narrows to 1.9 GHz at 30 GHz.

We show the dependence of the operational frequency on applied field in Figure 4. The dots represent the experimental results and the solid lines are the theoretical results based on Eq. (2) with no adjustable parameters. The dashed line represents the theoretical results in the absence of shape anisotropy. The effect of the shape anisotropy is clearly present in the experimental data, particularly at low magnetic fields. The effect is substantially larger in Fe than in Permalloy because the saturation magnetization in Fe is more than double that of Permalloy.

In summary we have designed and built a microstrip notch filter based on ferromagnetic metals. These devices show large attenuations with relatively low insertion loss. The growth and structuring of the filter is compatible with placing such a device on a chip with additional high frequency electronics. We also show that substantial increases in operational frequency can be achieved by using shape anisotropy of the ferromagnetic metal.

References:

1) Ernst Schloemann, Randal Tustison, Jehoshua Weissman, H. Jerrold Van Hook, and Thomas Varitimos, *J. Appl. Phys.*, vol. 63, pp. 3140-2, 1988

2) V. S. Liau, T. Wong, W. Stacey, S. Ali, and E. Schloemann *IEEE MTT-S*, vol. 3, pp. 957-60, 1991

3) C. S. Tsai, Jun Su, and C. C. Lee, IEEE Trans. Magn., vol. 35, pp. 3178-80, 1999

4) N. Cramer, D. Lucic, R. E. Camley, and Z. Celinski, *J. Appl. Phys.*, vol. 87, pp. 6911-3, 2000

5) N. Cramer, D. Lucic, D. K. Walker, R. E. Camley, and Z. Celinski IEEE Transactions on Magnetics, Volume: 37, 2392 (2001)

6) Bijoy Kuanr, L. Malkinski, R. E. Camley, and Z. Celinski and P. Kabos

J. Appl. Phys, Vol 93, 8591 (2003)

7) E. Salahun, P. Quéffélec, G. Tanné, A.-L Adenot, A.-L. and O. Acher, J. Appl. Phys. Vol 91, 5449 (2002)

8) I. Hunyen, G. Goglio, D. Vanhoenacker, and A. Vander Vorst, IEEE Microwave and Guided Wave Letters, Vol 9, 1051 (1999)

9) Y. Zhuang, B. Rejaei, E. Boellaard, M. Vroubel, and J. N. Burghartz, IEEE Microwave and Wireless Components Letters, Vol 12, 1531 (2002).

10) R. E. Camley and D. L. Mills, *J. Appl. Phys.*, vol. 82, pp. 3058-67, 1997

11) R. J. Astalos and R. E. Camley, *J. Appl. Phys.*, vol. 83, pp. 3744-3749, 1998

12) R. J. Astalos and R. E. Camley, Phys. Rev. B Vol 58 8648 (1988)

13) Roger B. Marks, IEEE Trans. MTT **39** 1205 (1991).

Figure Captions:

Figure 1 Structure of the microstrip notch filter.

Figure 2 Transmission parameter in the Permalloy-based notch filter as a function of frequency for different applied magnetic fields. Inset shows theoretical results.

Figure 3 Transmission parameter in the Fe-based notch filter as a function of frequency for different applied magnetic fields.

Figure 4 Frequency of attenuation dip as a function of applied field for Fe and Permalloy notch filters. Note the shape anisotropy produces a significant difference at low fields.
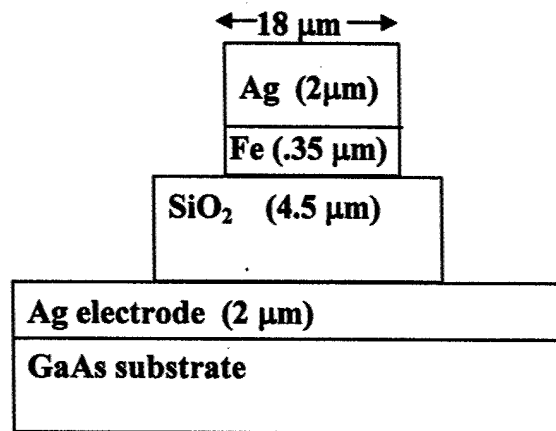
Figure 1: Structure of the microstrip notch filter.
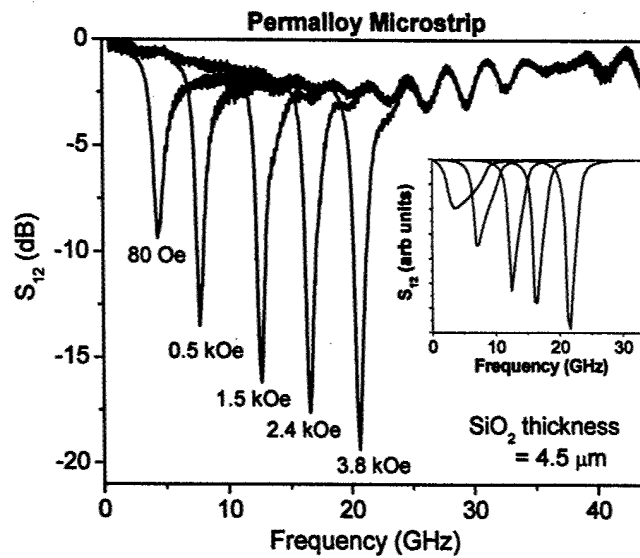
Permalloy Microstrip

Figure 2: Transmission parameter in the Permalloy-based notch filter as a function of frequency for different applied magnetic fields. Inset shows theoretical results.
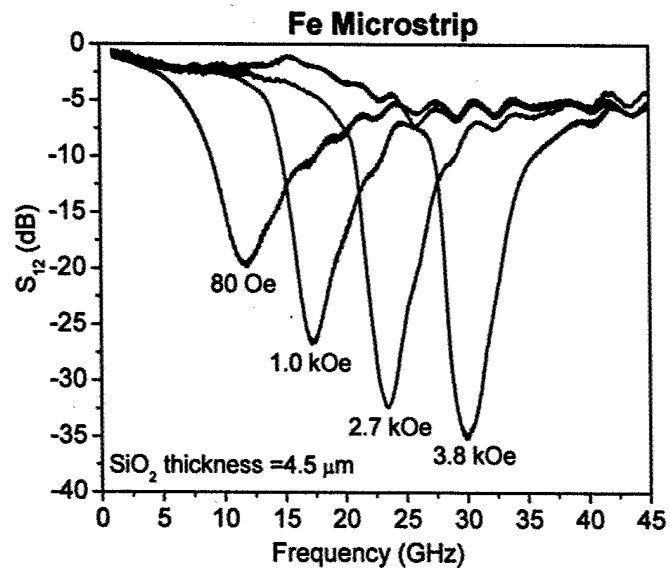
Figure 3: Transmission parameter in the Fe-based notch filter as a function of frequency for different applied magnetic fields.

Fe-based Microstrip

With shape anisotropy

No shape anisotropy

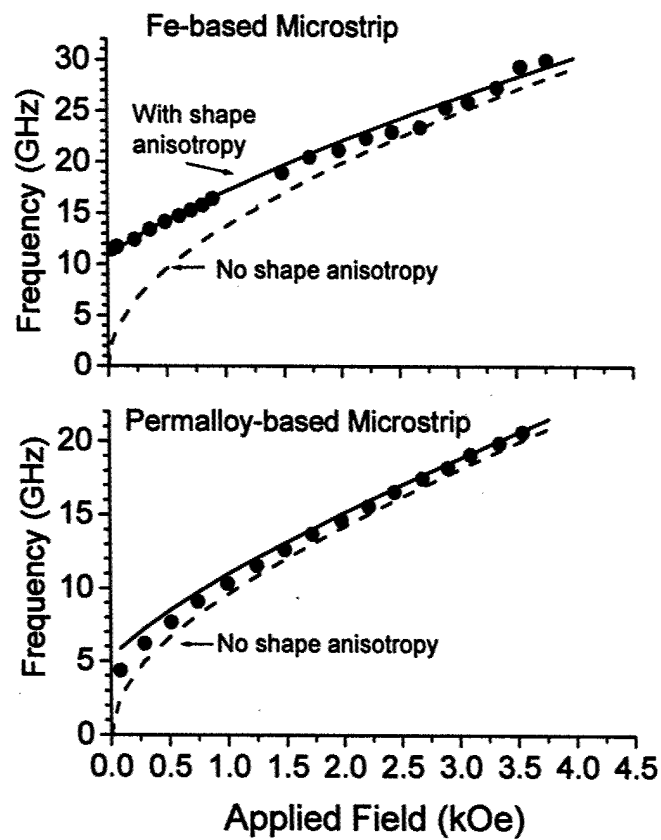**Permalloy-based Microstrip**

No shape anisotropy

Figure 4: Frequency of attenuation dip as a function of applied field for Fe and Permalloy notch filters. Note the shape anisotropy produces a significant difference at low fields.

Invention Disclosure Form

This form is used to report a discovery or invention made by faculty members, fellows, and staff members (including students on appointment as University employees), by anyone using University facilities, or by anyone collaborating with any of the above individuals ("Inventors"). Inventors at CU are bound by University of Colorado Policy on Discovery and Patents.

I. INVENTOR INFORMATION

Please print your name and sign where indicated.

A. Names of Inventors. List the corresponding inventor first. The corresponding inventor will be the point-of-contact between your research group and the Tech Transfer Office.

Corresponding Inventor
Name:____Zbigniew Celinski_____ Title:____Assoc. Professor_____
Telephone:__(719) 262-3583 _ E-mail:__zcelinsk@uccs.edu
Department:___Physics_____ Campus Address:__Colorado Springs____
Signature:_____ Date:_____

Inventor   Affiliation:_____
Name:___Robert Camley_____Title:_____Professor_____
Telephone:___ _(719) 262-3512 _____ E-mail:____ rcamley@uccs.edu_____
Department:__Physics_____ Campus Address:____ Colorado Springs____
Signature:_____ Date:_____

Inventor   Affiliation:_____
Name:_____ Title:_____
Telephone:_____ E-mail:_____
Department:_____ Campus Address:_____
Signature:_____ Date:_____

Inventor   Affiliation:_____
Name:_____ Title:_____
Telephone:_____ E-mail:_____
Department:_____ Campus Address:_____
Signature:_____ Date:_____

Attach additional inventor identification sheets as necessary.

II. INVENTION

Inventions include new processes, products, apparatus, compositions of matter, living organisms, or improvements to existing technology in those categories.

A. Invention Title. The title should be broad and non-confidential, i.e. what you can do, <u>not</u> how to do it.

A High Frequency Tunable Band Pass Filter Based on Thin Magnetic Films

B. Abstract (Non-confidential)

Most communication at long distances is done through the use of electromagnetic waves. Radio, for example, uses electromagnetic waves with frequencies from a few kilohertz to hundreds of megahertz. Recently cell phones and other technologies have been using higher frequencies in the one to two gigahertz range. Each of these frequency ranges requires different signal processing devices to capture and translate the signal and to separate one signal from another. The invention offers a filter which can be used to allow only certain frequencies to pass through and blocks signals at unwanted frequencies nearby. Furthermore the filtering region can be tuned over a wide range of frequencies (1 GHz to 40 GHz) by an external magnetic field and by choice of materials. The construction method allows this filter to be part of a high-frequency electronic system (semiconductor integrated circuit / filter) which should allow for mass production and use in small telecommunication devices. This filter may also be of use in military and commercial radar-like systems.

The invention is based on using a layered magnetic structure which is produced in a magnetron sputtering system. A particular advantage of this structure is that it does not need extreme quality magnetic materials in order to achieve the desired performance.
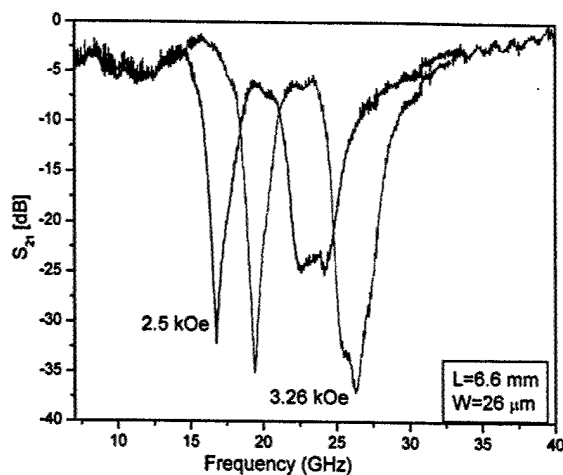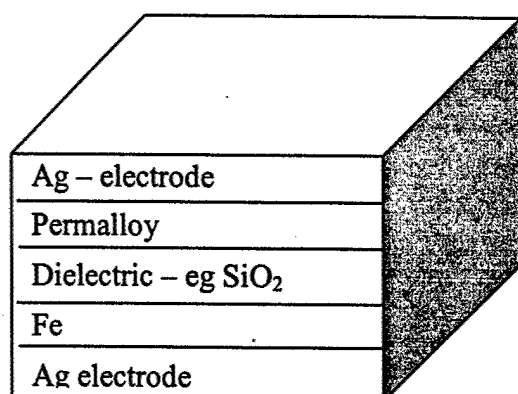
C. Confidential Description of the Invention (Attach additional sheets as necessary)

A Low-Field, Frequency-Tunable Band Pass Filter

A novel band pass filter can be constructed using a layered structure with at least two different magnetic materials. This filter should work in the 5-50 GHz range with external magnetic fields of under 10 kG.
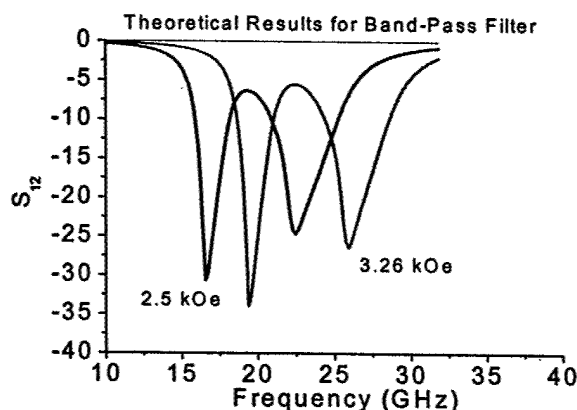
The key idea is that each of the magnetic materials will absorb electromagnetic waves at a different frequency. For example using Fe and Permalloy as the magnetic films and an external field of 2.5 kG one can have absorption bands centered at 17 GHz and 22 GHz. The region between these absorption bands has low attenuation and acts a band pass filter. This filter is tunable because an external magnetic field controls the position of the absorption bands.

One geometry for such a band pass filter is shown below. The thicknesses of the Fe and Permalloy are critical – The Fe thickness must be relatively small to minimize eddy current effects and is typically on the order of 0.15 micrometers. Because the Permalloy has a narrower linewidth and lower conductivity the thickness of the Permalloy should be substantially thicker than the Fe, typically 0.4 micrometers. Initial experimental results for this structure are shown below.

Ag – electrode
Permalloy
Dielectric – eg SiO_2
Fe
Ag electrode

We also have theoretical calculations for this effect. Using the same parameters as discussed above we find the results shown on the right. The between theory and experiment is excellent.

Other geometries are also possible. One can include additional magnetic layers and dielectric layers to improve the transmission in the band pass region and extend the band stop regions. Coplanar waveguides using two different magnetic materials are also possible.

Theoretical Results for Band-Pass Filter

D. Evidence for Patent. The criteria for a U.S. patent are novelty, non-obviousness, and utility. Please indicate below any evidence you have for, or evidence others might cite against, each criterion.

1. NOVELTY. In order for an invention to be patentable it must be new as defined in the patent law, which provides that an invention cannot be patented if the invention was previously known or used by others, or patented or described in a printed publication. How does your invention differ from what already exists? In what ways might it not be unique? **Please cite**

Most magnetic based filters are suitable for use in low frequency systems (below 3 GHz). A typical example is a filter based on the use of the insulator YIG (Yittrium Iron Garnet). To get to higher frequencies requires very large magnetic fields.

Our band-pass filter uses two different metallic based magnets and a layered structure which allows the filter to be useful at higher frequencies. Metallic magnets are seldom used in filters because of losses due to eddy currents. In very recent work magnetic metallic films have been used in band-stop filters which prevent transmission of electromagnetic waves at a particular frequency – in this case the high attenuation can be helpful. Our filter, in contrast, offers low attenuation in the band pass region and reasonable attenuation at nearby frequencies. Our structure allows many different magnetic materials to used which, in turn, allows better tailoring of the device to particular needs in terms of attenuation and frequency ranges.

2. NON-OBVIOUSNESS.
Even if the subject matter sought to be patented is not exactly shown by the prior art, and involves one or more differences over the most nearly similar thing already known, a patent may still be refused if the differences would be obvious to a person having ordinary skill in the area of technology related to the invention. Why is your invention not obvious?

Our filter is substantially different from previous systems. The nonobviousness is based on the unusual combination of techniques which are necessary for successful operation.

1) It is not obvious that one can create a band-pass filter by using two different magnetic materials in a way that is more typical for band-reject filters. The layering pattering necessary for good performance is also not obvious.

2) The thicknesses of the magnetic and dielectric layers have to be carefully designed in order to get a narrow band-pass frequency region and larger band-reject frequency regions nearby.

3) Previous work was based on an idea that the magnetic film needed to have exceptionally high magnetic quality – linewidths in YIG filters are on the order of 1-10 Oe. The design of the band-pass filter allows materials with substantially lower quality (linewidths up to 200 Oe) to be used. This has two advantages – growth and processing techniques can be compatible with typical industrial standards in the semiconductor industry and materials such as iron and Permalloy may be used (instead of YIG) and provide higher operational frequencies.

3. UTILITY. Who might find your invention useful, and why? What companies might be interested in making or selling it, and why? Is there other technology that currently provides similar utility? If so, what is the unique advantage of your invention?

There are a number of possible military and civilian applications. For example, the military has a need to see through fog, clouds and smoke. These obstacles are transparent for particular frequencies in the 20 – 100 GHz range. Thus signal processing in this range is of significant importance. There are obvious civilian uses as well, for example tracking and landing planes in severe weather conditions. Also, cell phones are now starting to use higher frequencies (in the several GHz range) and in order to separate one channel from another it might be useful to have a band pass filter as described here.

D. Stage of Development. Provide the date of conception and how it is documented. To what extent has the invention been realized <u>in practice</u>? In the case of biotech/pharmaceutical development, has the development been tested ___ in vitro; ___ in vivo (animal model(s): _____; Phase ___ Clinical Trials; other _____?

The idea of the invention was developed in May 22 2003.

Theoretical calculations were begun on June 9, 2003 and an initial version completed by July 4, 2003.

Initial experimental results showing proof of principle were available by July 9, 2003. A good experimental device was completed by Aug 7 2003.

E. Expert Opinions. Suggest experts who can provide an objective opinion of the merits of the invention, especially in view of its commercial potential. Please provide contact information.

Name: Dr. Pavel Kabos (National Institute of Standards and Technology, Boulder (303) 497-3997)
Dr. Mikael Ciftan   (US Army Research Office) (919) 549-0641

III. PUBLIC DISCLOSURE

Prior to filing for patent protection, public disclosure (a published paper, a widely available enabling abstract, or an offer for sale) may compromise patent rights. Upon disclosure, US patent law provides a one year grace period in which to file; however, essentially all foreign rights are lost. Inventors are urged to use discretion, take advantage of Confidential Disclosure Agreements available from this office, and file invention disclosures with the University well in advance of presentations or publications.

A. Has your invention been disclosed in an abstract, paper, talk, news story, thesis, or public conversation? If so, please list and enclose copies, if available.

No

B. Is a publication or other disclosure planned in the next six months? If so, please list
and enclose copies, if available.

Publication of the results are likely within the next six months. Manuscript is not
currently available.

**C. Have you sold or offered for sale any products that embody your invention?
Have you allowed others outside the University to use your invention?** If so, please
describe the circumstances and give dates.

No

**D. Has material related to the invention, i.e. reagents, biologicals, software, etc, ever
been sent to or received from another organization?** If so, give details (what was
transferred, date, receiving organization).

No

IV. SPONSORSHIP
Do not leave this section blank. If there were no external sponsors, please indicate.

Sponsoring agencies may require the University to disclose inventions that arise from funded
research.

A. Government Agency Contract / Grant No. / Title / PI.

US Army Research Office – Grants DAAD19-00-1-0146 and DAAD19-02-1-0174

B. Other Sponsoring Entity, including Cooperative Research Centers. Please give
name(s) of industry, university, foundation, I/URC, or other sponsor(s) and their university account number
and effective date(s).

AFOSR F49620-03-1-0207 (Subaward from NISSC)

C. Has your invention been disclosed to government or industry sponsors? If so, please provide details, including the names of organizations and their representatives.

Yes – results have been shown via e-mail to Mikael Ciftan of the US Army Research Office.

D. Related consulting agreements.